Seismic Design and Performance of Buckling Restrained Braced Frames with Eccentric Brace Configurations Part 2: Analysis Studies and Design Implications

CHAO-HSIEN LI, PAUL W. RICHARDS, and BRANDT W. SAXEY

ABSTRACT

This is the second of two companion papers discussing the seismic design and performance of buckling-restrained braced frames (BRBFs) with braces oriented in eccentric configurations. The companion paper (Li et al., 2026) introduces the proposed design procedures for the BRBFs with eccentricities and presents the elastic design results of nine case study buildings representing two building heights (12- and 3-story), two bracing configurations (chevron and single-diagonal), and various eccentricities. This paper first presents nonlinear response history analysis (NLRHA) results for the nine design case study buildings subjected to 16 ground motions scaled to the design basis earthquake (DBE) and maximum considered earthquake (MCE) levels. The analytical results demonstrate that BRBFs with eccentricities equal to twice the beam depth—double the current code limit of one beam depth—perform satisfactorily under seismic loading, provided they are properly capacity designed to account for brace eccentricities. The paper explores the relationship between brace eccentricity and key response parameters. The NLRHA results also validate the accuracy of the proposed analysis methods in estimating beam force demands in capacity design. Subsequently, nonlinear pushover analysis results for specific stories in selected chevron design cases are presented, with a focus on the effects of connection geometry, specifically combined and split gusset configurations, on local stress state in the beam region, analyzed through detailed finite element modeling. Lastly, the NLRHA results suggest that intentionally introducing brace eccentricities in single-diagonal BRBFs could potentially lead to more economical designs with enhanced seismic performance (e.g., reduced residual story drifts) as compared to concentric frames. Accordingly, design implications for single-diagonal eccentric BRBFs are explored, particularly concerning column capacity design with moment demands and the approximate story drift distribution for preliminary brace sizing.

Keywords: buckling restrained braced frames, eccentric bracing, eccentric braced frames.

INTRODUCTION

Buckling-restrained braced frames (BRBFs) are primarily used in concentric configurations as the AISC *Seismic Provisions* (2022a) limit eccentricities in BRBFs to less than a beam depth. However, architectural needs, like doorways or corridors, may require eccentric bracing. If the eccentricity exceeds a beam depth, additional columns can be added to meet the requirements of the AISC *Seismic Provisions*, but these added columns affect the cost and architecture. Several previous analytical studies (Hosseini and Amiri, 2017; Lejano and Mas, 2017; Prinz and Richards, 2012; Shakib and Safi, 2012; Vayda, 2015) demonstrated the feasibility of BRBFs in eccentric configurations without adding columns, although this can result in reduced cost effectiveness in cases of large eccentricities.

Recent research also highlights that BRBFs with eccentricities, besides offering architectural benefits, may help control residual drifts during seismic events. Gholami et al. (2021) investigated BRBFs with eccentricities as a means for controlling residual drift but only found them particularly effective when used in parallel with post-tensioned frames. Hariri and Christopoulos (2024) investigated BRBFs that are configured to induce beam bending and found they were able to limit residual drifts to 0.5% or less.

This study investigates the seismic design and performance of BRBFs with eccentricities and is presented in two companion papers. Part 1 (Li et al., 2026) presents design procedures and analysis methods for capacity design of the beams and columns in BRBFs with eccentricities and then presents design results for nine case study BRBFs (see Figure 1) with eccentric or concentric bracing configurations. This paper, Part 2, presents the analytical studies for evaluating the seismic performance of these case study designs.

Figure 1 shows BRBF designs for nine archetypes adapted from NIST GCR 10-917-8 (2010). The archetypes featured two heights (12- and 3-story), two bracing configurations

Chao-Hsien Li, Senior Research Engineer, CoreBrace, LLC, West Jordan, Utah. Email: chaohsien.li@corebrace.com

Paul W. Richards, Associate Professor, Brigham Young University, Provo, Utah. Email: paul.richards@byu.edu (corresponding)

Brandt W. Saxey, Technical Director, CoreBrace, LLC, West Jordan, Utah. Email: brandt.saxey@corebrace.com

Paper No. 2024–19R

(chevron and single-diagonal), and various eccentricities. In Figure 1, the BRBF design cases are grouped into four categories: 12S-CH, 12S-SD, 3S-CH, and 3S-SD. The prefixes 12S and 3S denote the 12-story and 3-story heights, respectively, while the suffixes CH and SD refer to the chevron and single-diagonal bracing configurations in the BRBFs. Each group includes two cases: one concentric (C) and one eccentric (E2d), with the eccentricity of twice the nominal beam depth (21 in.) of W21 beams. Group 12S-CH, also has an additional case (E1d) with an eccentricity equal to the beam depth. The E2d cases exceed the AISC *Seismic Provisions* limit (2022a), while the E1d case meets the code's maximum eccentricity allowance. Design cases are named using the group name and eccentricity condition (see Figure 1).

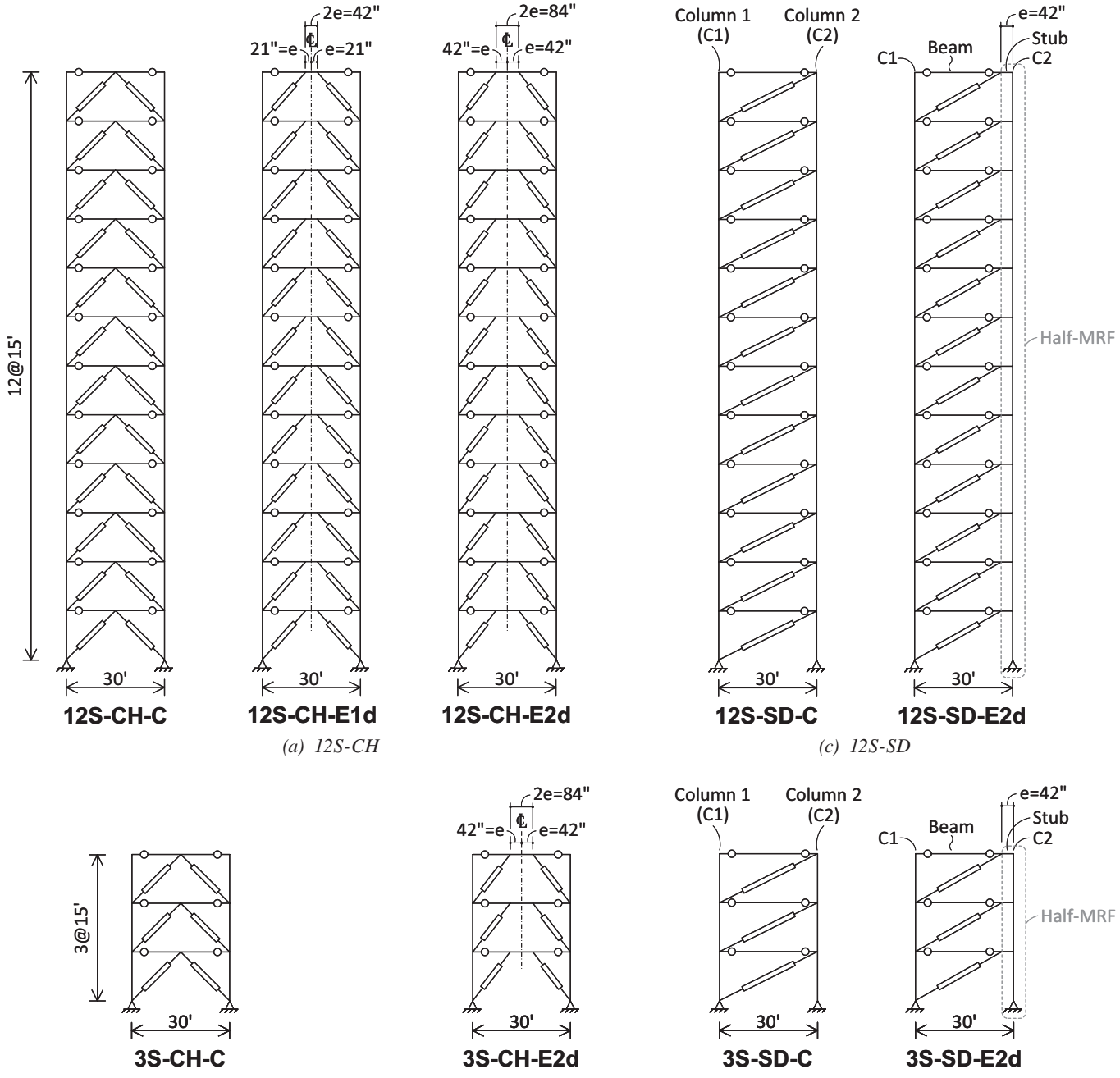

Fig. 1. Frame elevations for BRBF case designs.

This Part 2 paper first presents a nonlinear response history analysis (NLRHA) of the seismic performance for the nine design cases. It then discusses nonlinear pushover analysis results for specific stories, focusing on the effects of connection geometry through detailed finite element modeling. Lastly, design implications for single-diagonal eccentric BRBFs are explored.

RESPONSE HISTORY ANALYSIS STUDY

Overview

Nonlinear response history analysis (NLRHA) was used to investigate the response of the case study buildings and validate the proposed design procedure. A suite of 16 historical ground motion records were selected and scaled to design basis earthquake (DBE) and maximum considered earthquake (MCE) levels, which were used as the input motions for NLRHA. The mean structural responses (such as peak story drifts, peak brace core strains, etc.) averaged from the 16 ground motions are reported in this section.

Modeling

OpenSees (Mazzoni et al., 2006) was used to create nonlinear models for the BRBFs in this study. Individual BRBFs were modeled and tied to a fishbone system (Lignos et al., 2013) to represent the gravity framing, including lateral stiffness of the gravity beam-to-column connections [Figure 2(a)]. Gravity loads and seismic masses were applied to the fishbone system. For the BRBF portion of the models (BRBF-C and BRBF-E), beam-to-column intersections were modeled as rigid joints (representing gusset plates), and pins were introduced in the beam outside the connections (representing bolted connections) [Figure 2(a)]. Offset elements were used to model the stiffened regions inside of panel zones and locations of corner gussets. Offsets regions were assigned 10 times the elastic flexural properties of the members framing into centerline nodes. Base connections were modeled as pinned.

BRBF beams and columns were modeled with elastic beam-column elements, and the member forces in these elements were evaluated using NLRHA to confirm that forces did not exceed elastic limits. BRBF beams were pinned outside of the gusset region [Figure 2(a)]. Resistance provided by simple gravity connections [within the fishbone frame shown in Figure 2(a)] was modeled using nonlinear hinges representing lumped properties of gravity shear tab connections in the part of gravity system tributary to the BRBFs. These gravity connections were modeled using the Pinching4 material (Lowes et al., 2003) with parameters calculated according to ATC-114/NIST guidelines (Liu and Astaneh-Asl, 2000, 2004; NIST, 2017).

Buckling restrained braces (BRBs) were modeled as corotational truss elements (using workpoint-to-workpoint length, L_{WP}) with a hysteretic behavior defined by a Menegatto-Pinto steel material (SteelMPF) with isotropic strain hardening. Initial stiffness of the BRBs was defined by the effective stiffness factor, KF [see Tables 4–7 in Part 1 (Li et al., 2026)] using the bay geometry and L_{WP}. Cyclic properties of BRBs were calibrated to match the ultimate strength for both tension (P_{uT}) and compression (P_{uC}) at the expected deformation at a 2% story drift, aligning with the experimental brace response per the AISC *Seismic Provisions* (2022a) loading protocol. BRBs were modeled and calibrated using an expected core yield strength, $P_{ysc,exp}$, of 42 ksi. An illustration of a calibrated BRB material and backbone targets is shown in Figure 2(b).

Models included second-order effects both locally on the braced frame and through the leaning column as part of the fishbone gravity framing model. Inherent viscous damping was included as 2% Rayleigh damping at the first- and third-mode periods. Mass proportional damping was applied to all nodes, but stiffness proportional damping was only assigned to linear elastic elements.

Modal Results

Tables 1 and 2 summarize the OpenSees (Mazzoni et al., 2006) modal analysis results for the 12-story and 3-story design cases, respectively. The structural periods for the first three modes and the associated cumulative modal mass participation ratios, Γ_{cum}, are reported. From the period variations between the design cases in Group 12S-CH or 3S-CH, it can be seen that the structural period increases with the eccentricity, indicating the decreasing frame lateral stiffness with the eccentricity for the chevron BRBFs since all the design cases in the same groups carry identical seismic masses. By contrast, for the single-diagonal BRBFs (Groups 12S-SD or 3S-SD), the analysis results show a trend that the structural period decreases (i.e., the frame lateral stiffness increases) with the eccentricity. The half-moment resisting frame (half-MRF), formed by the stubs and the adjacent columns [i.e., Column 2 (C2) members] as shown in Figures 1(c) and 1(d) (see also Figure 17), in the single-diagonal eccentric frames provides extra lateral stiffness to the system despite the decreasing stiffness provided by the braces as the eccentricity increases. The contribution from the half-MRF leads to an increasing total lateral stiffness with the eccentricity for the single-diagonal BRBFs.

Ground Motions Selection and Scaling

Sixteen ground motion records selected from the FEMA P-695 far-field set (ATC, 2009) were used for NLRHA in this study (see Appendix). The target spectral shape for

scaling ground motions was the design spectrum prescribed by SEI/ASCE 7, *Minimum Design Loads and Associated Criteria for Buildings and Other Structures* (ASCE, 2022), with S_{DS} = 1.0g and S_{D1} = 0.6g, which is consistent with that employed for the three design cases in this study. As shown in Figure 3, the suite of selected ground motions was scaled such that the average of the 5% damped spectra does not fall below 90% of the target response spectrum over the code-prescribed period range (ASCE, 2022). The averaged 1st-mode and 3rd-mode periods (denoted as $T_{1,avg}$ and $T_{3,avg}$, respectively) of the OpenSees models (Mazzoni et al., 2006) in 12-story or 3-story design case groups were used to determine the period range. The upper bound of the period range was set at $2T_{1,avg}$, while the lower bound was set at the lessor between $0.2T_1$,avg and $T_{3,avg}$ to ensure the period range includes at least the number of modes necessary to achieve 90% mass participation. Each ground motion was scaled to both design basis earthquake (DBE) and maximum considered earthquake (MCE) levels. While NLRHA was conducted for both levels, the results presented in this paper focus on the MCE-level responses, obtained from the peak structural responses averaged across the suite of MCE ground motions.

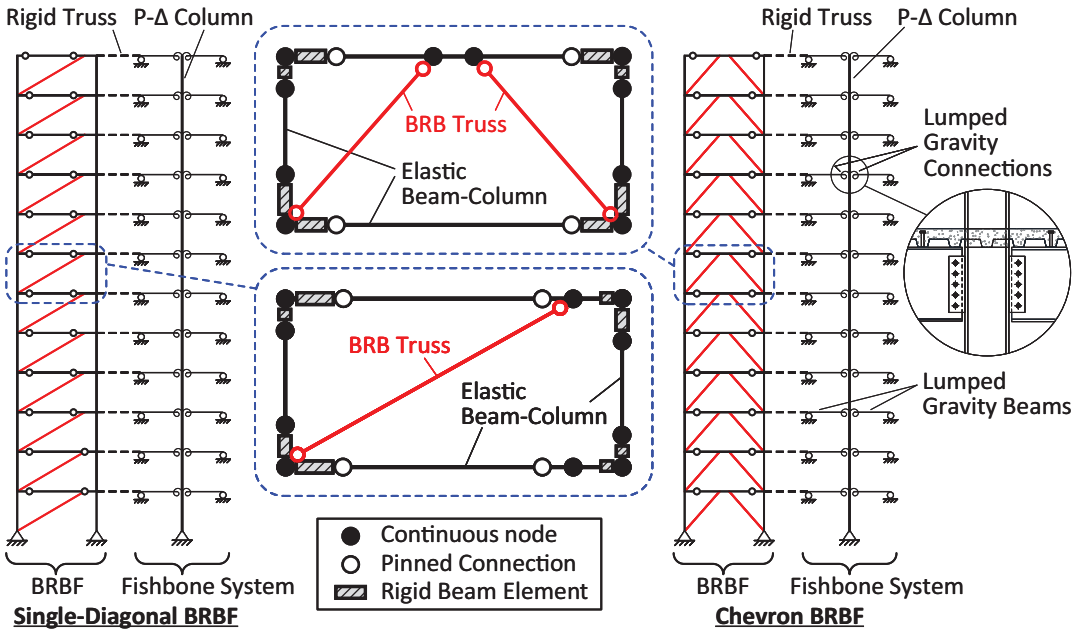

(a) Elements and constraints

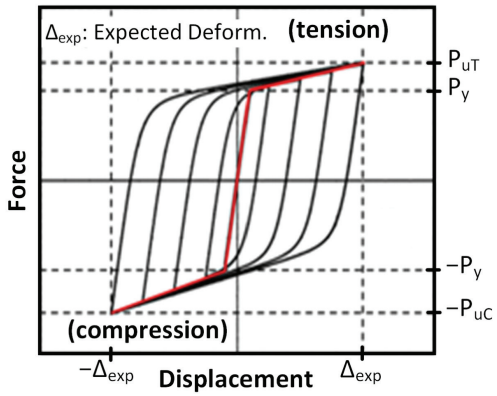

(b) Example of BRB modeling and calibration

Fig. 2. OpenSees modeling methods.

Table 1. Modal Analysis Results for 12-Story BRBF Design Cases										
Mode	Group 12S-CH						Group 12S-SD			
	12S-CH-C		12S-CH-E1d		12S-CH-E2d		12S-SD-C		12S-SD-E2d	
	Period (s)	Γ_{cum}	Period (s)	Γ_{cum}	Period (s)	Γ_{cum}	Period (s)	Γ_{cum}	Period (s)	Γ_{cum}
1	2.920	71.3%	2.972	72.5%	3.081	73.8%	3.228	73.6%	3.043	72.9%
2	0.975	89.4%	1.015	89.5%	1.075	89.7%	1.086	89.8%	1.015	89.8%
3	0.546	94.4%	0.567	94.3%	0.610	94.5%	0.610	94.3%	0.569	94.4%

Table 2. Modal Analysis Results for 3-Story BRBF Design Cases								
Mode	Group 3S-CH				Group 3S-SD			
	3S-CH-C		3S-CH-E2d		3S-SD-C		3S-SD-E2d	
	Period (s)	Γ_{cum}	Period (s)	Γ_{cum}	Period (s)	Γ_{cum}	Period (s)	Γ_{cum}
1	0.793	86.3%	0.895	86.9%	0.918	85.9%	0.896	87.4%
2	0.308	97.7%	0.352	97.9%	0.340	97.5%	0.340	98.3%
3	0.183	99.9%	0.192	100.0%	0.193	99.8%	0.202	99.8%

Analysis Results

Story-Drift Response

Story-drift results from the NLRHA analyses are summarized in Figures 4, 5, and 6. For DBE loading, the peak interstory drift ratios were similar among the cases in each group [see Figures 4(a), 4(b), 4(c), and 4(d) for Groups 12S-CH, 3S-CH, 12S-SD and 3S-SD, respectively], with values less than 0.02 rad, consistent with the design intent. For chevron BRBFs under MCE loading [see Figures 5(a) and 5(b) for Groups 12S-CH and 3S-CH, respectively], the story-drift response generally increases with the eccentricity in the lower stories, where the largest story drifts along the building height took place. However, the interstory drift of some intermediate stories in the 12-story eccentric frames (Cases 12S-CH-E1d and 12S-CH-E2d) were less than those in the eccentric frame (12S-CH-C), as shown in Figure 5(a).

On the other hand, for single-diagonal BRBFs, the peak story-drift response generally decreases with brace eccentricity. For 12-story design cases [Figure 5(c)], the MCE-level

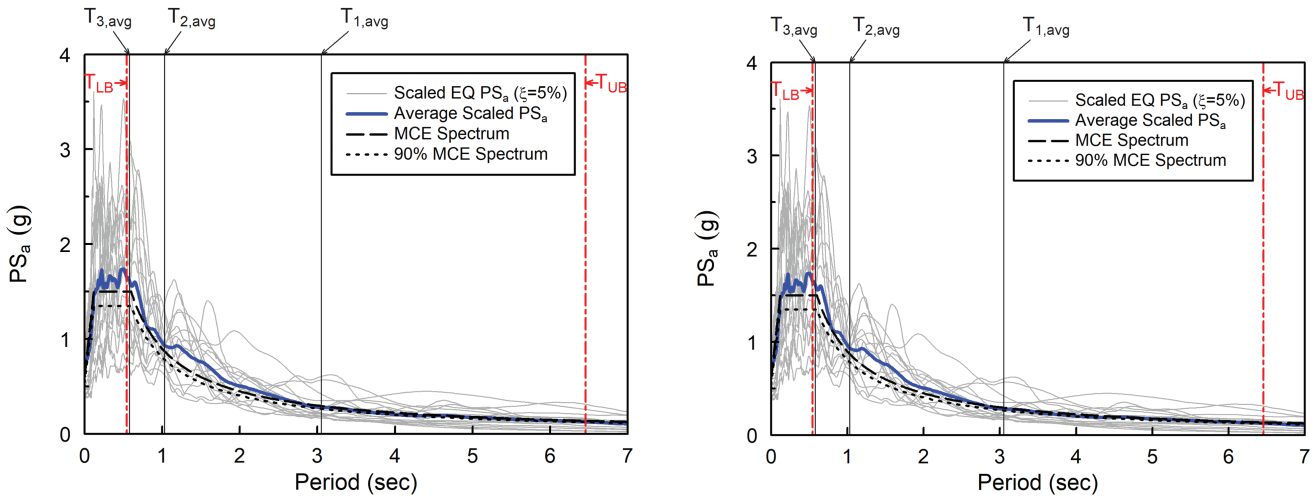

(a) For 12-story BRBF models *(b) For 3-story BRBF models*

Fig. 3. Pseudo-acceleration spectra of MCE-scaled input ground motions used for analyses.

story-drift response in the eccentric Case 12S-SD-E2d was noticeably less than that in the concentric case 12S-SD-C for the lower half of the frame. For 3-story design cases [Figure 5(d)], the MCE-level story drifts in 3S-SD-E2d were also smaller than those in 3S-SD-C, although to a smaller degree. The reduced drifts in the single-diagonal eccentric BRBFs could be attributed to the fact that the half-MRF [see Figures 1(c) and 1(d)] serves as an elastic backup lateral system, providing stiffness after the braces yield, leading to a reduction on the inelastic story drift of the frame.

It is noted that, in Figures 5(c) and 5(d), there are two additional curves, 12S-SD-E2d* and 3S-SD-E2d*, respectively representing alternative designs for Cases 12S-SD-E2d and 3S-SD-E2d in which an alternate method for column design is considered. In contrast to the proposed design for 12S-SD-E2d and 3S-SD-E2d, where Column 2 (C2) shears are considered, the alternative designs for 12S-SD-E2d* and 3S-SD-E2d* follow the practice of assuming the entire story shears are carried by the braces only. Hence, the conventional practice considered in the alternate design would lead to conservative design results. All the member sizes for the braces, beams, and columns in Cases 12S-SD-E2d* and 3S-SD-E2d* are larger than those in 12S-SD-E2d and 3S-SD-E2d, respectively. As reported in Part 1, the alternative designs are 4% to 6% heavier. As shown in Figures 5(c) and 5(d), the alternative design Cases 12S-SD-E2d* and 3S-SD-E2d* generally had smaller story-drift response than 12S-SD-E2d and 3S-SD-E2d.

Furthermore, Figure 5 shows that the MCE-level peak story drifts in all design cases for both chevron and single-diagonal configurations were less than the associated code-prescribed story-drift limits (0.04 and about 0.034 rad for the 3-story and 12-story design cases, respectively), determined in accordance with ASCE/SEI 7 and based on the full height of building. This confirms the feasibility and satisfactory seismic performance of the eccentric BRBFs.

Figure 6 shows the residual story drift response after the MCE loading. For Group 12S-CH design cases [Figure 6(a)], it is seen that the residual story drifts in the lower stories of the eccentric Cases 12S-CH-E1d and 12S-CH-E2d were noticeably higher than those in the concentric

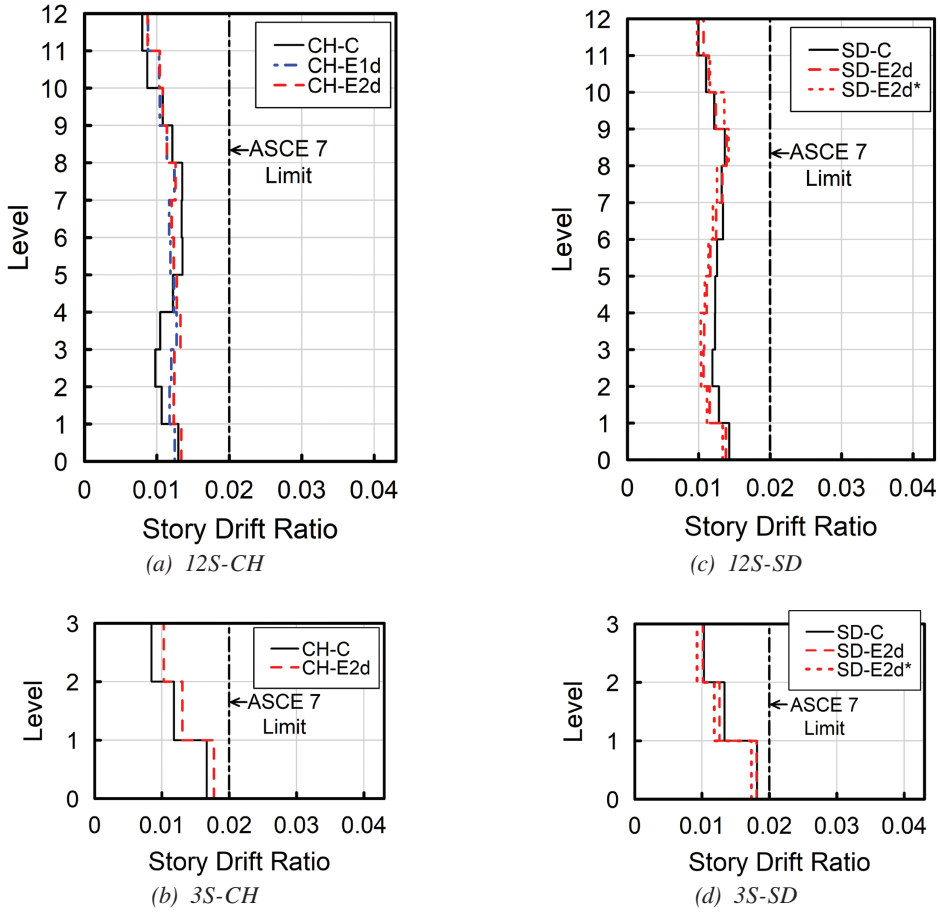

(a) 12S-CH *(c) 12S-SD*

(b) 3S-CH *(d) 3S-SD*

Fig. 4. DBE-level peak story drifts (mean of maximums).

Case 12S-CH-C. Also, the response in 12S-CH-E2d was generally higher than 12S-CH-E1d. For Group 3S-CH [Figure 6(b)], the residual story drifts in 3S-CH-E2d were slightly higher than those in 3S-CH-C, despite similar response in the first story for both cases. To summarize, analysis results show that for chevron BRBFs, the residual story drifts generally increase with brace eccentricity.

In contrast to the chevron BRBFs, the eccentric single-diagonal BRBFs had noticeably smaller residual response compared to the corresponding concentric frames. As shown in Figure 6(c), the residual story drifts in 12S-SD-E2d were significantly lower than those in 12S-SD-C for the lower stories of the building. For 3-story design cases [Figure 6(d)], all the residual story drifts along the entire building heights in 3S-SD-E2d were less than those in 3S-SD-C. Furthermore, as shown in both Figure 6(c) and Figure 6(d), the alternative design cases 12S-SD-E2d* and 3S-SD-E2d*, with the associated heavier frame members, had further reduced residual story drift response.

In summary, these analysis results suggest that using eccentric configurations for single-diagonal BRBFs would be an efficient way to reduce story drifts, especially residual drifts. It is noted that, based on the design procedure proposed in this study, the eccentric Cases 12S-SD-E2d and 3S-SD-E2d were even lighter than the corresponding concentric frames by about 3% and 5%, respectively (see Part 1 for details) while achieving a better control of the story-drift response. When the conventional, but conservative, design practice is used, the eccentric Cases 12S-SD-E2d* and 3S-SD-E2d* had further enhanced seismic performance in controlling the story drift with only a modest increase in weight [about 6% and 4%, respectively (see Part 1 for details)].

Brace Response

Plots of peak BRB core strains from the NLRHA analyses at MCE level are shown in Figure 7. The peak BRB strains are within the expected values corresponding to a story drift ratio of 0.02, as listed in Part 1 Tables 4 through 7 (Li et al., 2026), at all levels except for the bottom three stories in the 12-story cases [Figures 7(a) and 7(c)] and for the ground floor in the 3-story cases [Figures 7(b) and 7(d)]. The higher strains (2.44% maximum) at these bottom levels

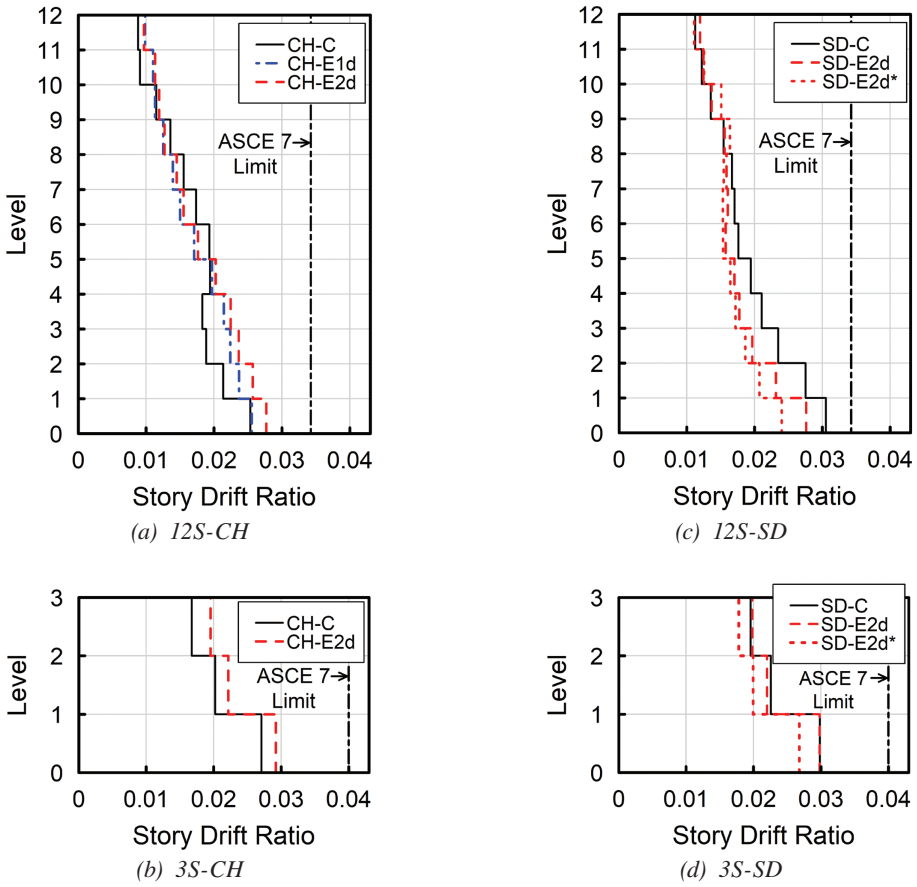

Fig. 5. MCE-level peak story drifts (mean of maximums).

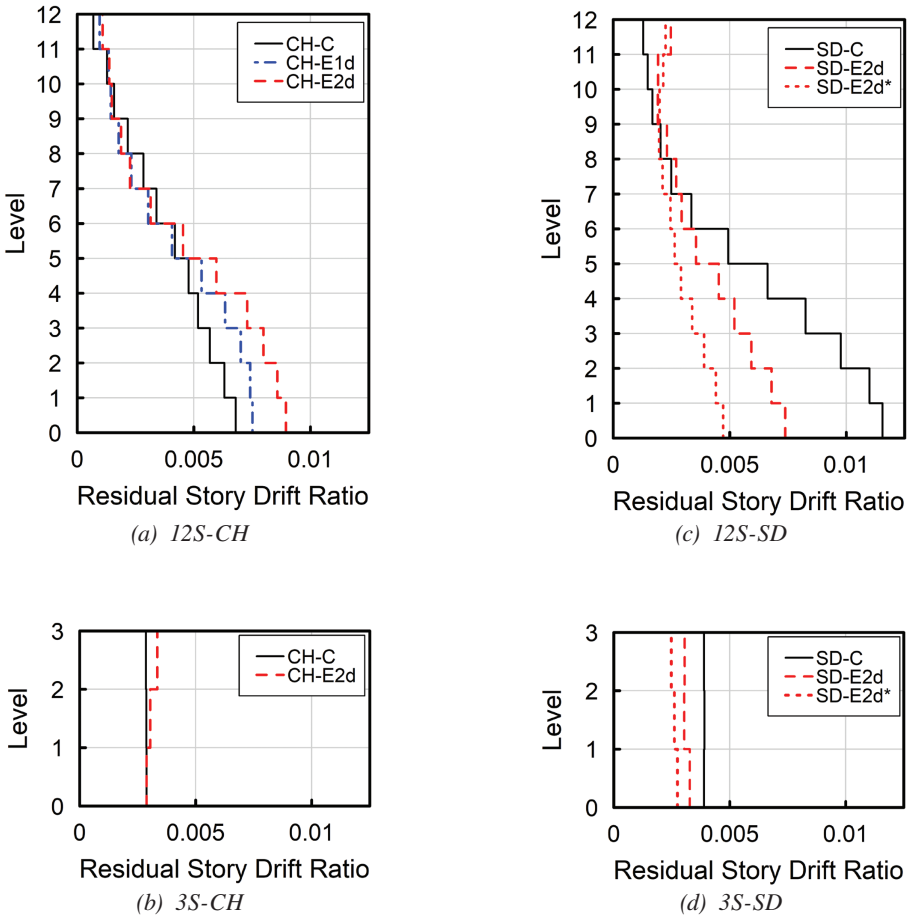

(a) 12S-CH *(c) 12S-SD*

(b) 3S-CH *(d) 3S-SD*

Fig. 6. MCE-level residual story drifts (mean of maximums).

remain, however, within the experimental BRB deformation capacities (which typically achieve at least 3% strain). For comparison between eccentric and concentric frames, there seems to be a trend that the eccentric frames generally develop BRB core strains somewhat higher than the concentric frames, at least for those braces experiencing the highest strains. For Groups 12S-SD, 3S-CH, and 3S-SD, the eccentric frames had almost all BRB strains higher than the corresponding concentric frames. For Group 12S-CH [Figure 7(a)], the two eccentric frames (12S-CH-E1d and 12S-CH-E2d) developed higher BRB core strains at the bottom four stories, where the largest overall BRB strains were seen, than in the concentric case (12S-CH-C) with smaller core strains at the upper stories.

BRB normalized ultimate force represents the ratio of the maximum compressive force, P_u, in a BRB from the NLRHA to its expected yield force, P_{ye}, which is the multiplication of yielding core area, A_{sc}, and the expected yield stress, $F_{ysc,\text{exp}}$. It is a measure of the overstrength, ωβ, seen in the BRB, where ω is the strain-hardening adjustment factor, and β is the compression strength adjustment factor. The plots of the analytical peak BRB normalized forces at MCE levels are provided in Figure 8. BRBs were modeled as having a $F_{ysc,\text{exp}}$ of 42 ksi, and as such, this normalized force is only a measure of the strain hardening and compression overstrength that develops and does not include any material overstrength that would exist when a material yield stress range ($F_{ysc,\text{min}}$ to $F_{ysc,\text{max}}$) is allowed for. Because the brace overstrength is dependent on the core strain response, similar trends are observed between the BRB core strains and normalized ultimate forces. They include that the BRB normalized ultimate forces are within the expected overstrength ωβ values [see Tables 4 through 7 in Part 1 (Li et al., 2026)] except for the bottom three stories in the 12-story cases [Figures 8(a) and 8(c)] and for the ground floor in the 3-story cases [Figures 8(b) and 8(d)], where the observed overstrength in the first story exceeded the expected values by about 9.7% and 12.4% for 12-story and 3-story cases, respectively.

In addition, the eccentric BRBFs generally developed slightly higher brace overstrength than the corresponding concentric frames did. It should be noted that while the story drifts considerably exceeded 2% as seen in Figure 5 by as much as 50%, the resulting overstrength only

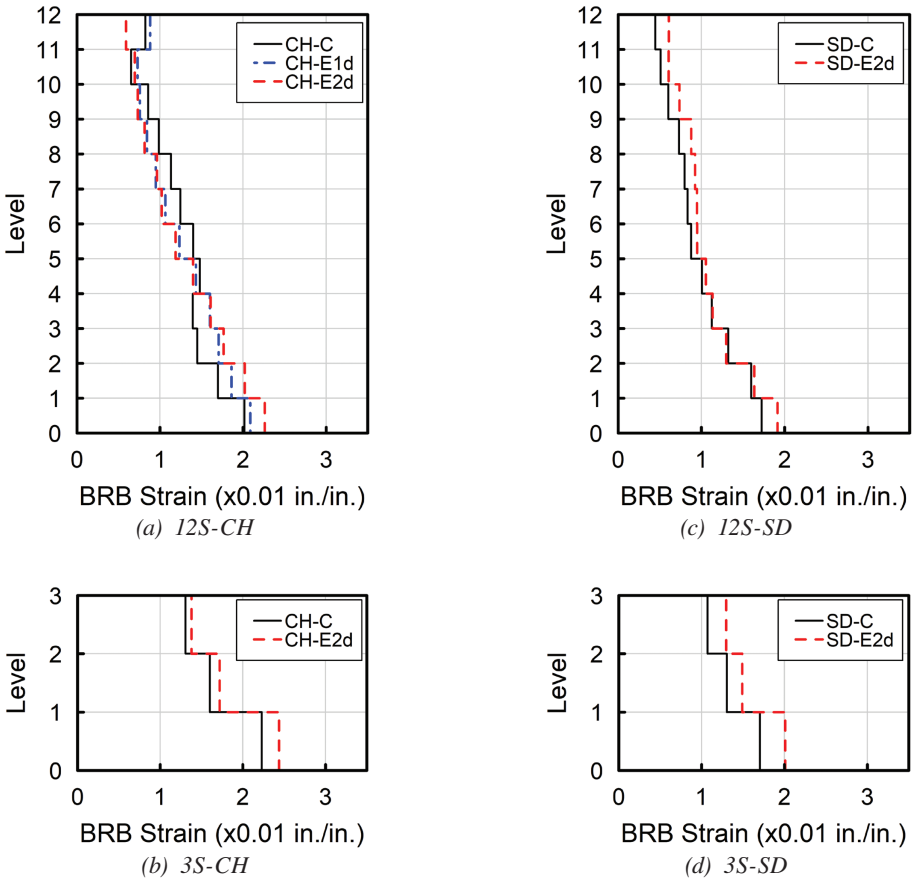

Fig. 7. MCE-level peak BRB strains (mean of maximums).

exceeded the values expected at 2% by a small amount. A similar statement about the resulting core strain is also true. These facts speak to the large total strain ranges experienced in AISC testing protocols relative to the generally lower total strain ranges seen in earthquake records even with higher absolute reference strains.

Beam Member Forces

To validate the beam capacity design methods proposed in Part 1 (Li et al., 2026) for BRBFs with eccentricities, selected beam member force diagrams from an NLRHA for 12-story design cases were plotted in Figures 9 and 10. These diagrams, showing beam member forces at a story-drift ratio of 0.02, are compared with the estimates from the proposed methods. Note that the 0.02 drift ratio was used to set brace overstrength factors (ω and β), which were used to estimate brace forces in the BRBF capacity design. The input motion for selected NLRHA is from the north-south component of the 1994 Northridge earthquake (Canyon Country–W Lost Cany), scaled to MCE level. The analysis with this ground motion was chosen because it produced peak drift ratios of about 0.02 in the lower three stories of all 12-story cases.

Figure 9 presents beam member force diagrams from the 12-story chevron BRBF design cases. The beams on the 2nd, 3rd, and 4th floors were selected for Cases 12S-CH-C, 12S-CH-E1d, and 12S-CH-E2d, respectively, because the braces beneath these beams are identical in size (A_{sc} = 5.5 in.^{2}). The consistent brace sizes were chosen to ensure comparable forces on the selected beams, clearly illustrating how beam forces are influenced by brace eccentricity without being affected by variations in brace force. The forces are shown at point in time when the story below each beam reached about 0.02 rad drift.

In each subfigure displaying the member forces, both the response from the NLRHA (represented by a solid line) and the estimated force diagrams, calculated using the proposed analysis methods, are shown. The estimates are depicted as dashed lines and labeled as Est. For discussion purposes, two sets of estimated member forces are presented in Figure 9: one due to seismic effects only, labeled Est. (E), and the other due to the combined seismic and gravity effects, labeled Est. (E+G). For the shear and moment diagrams,

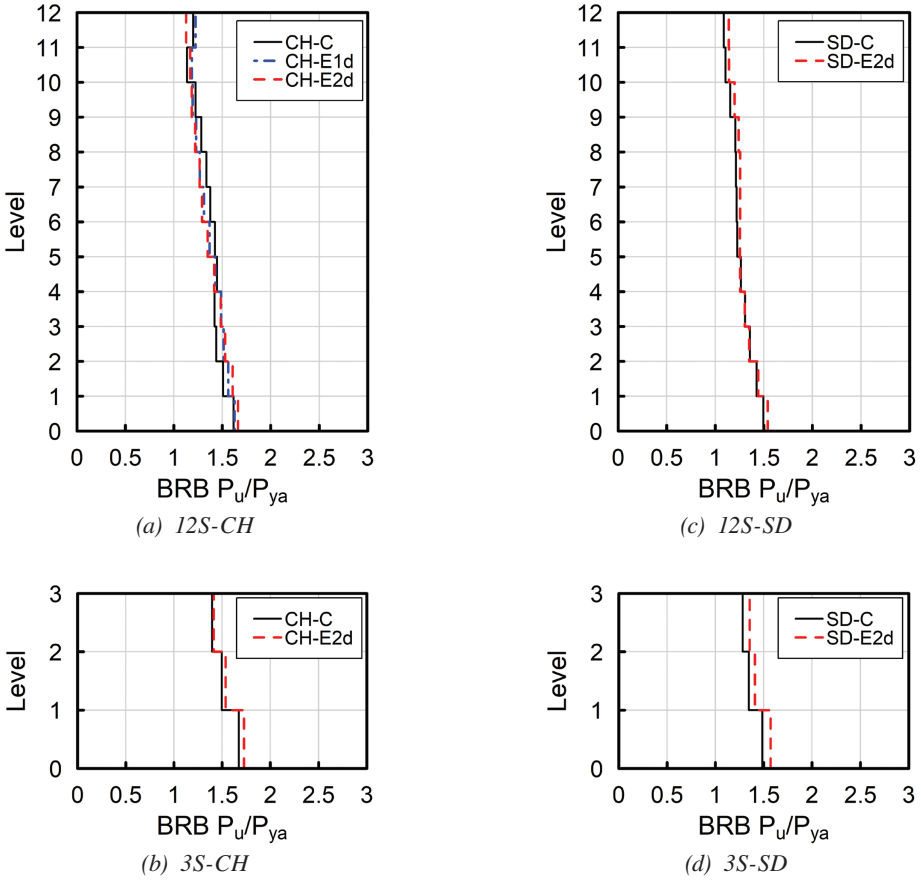

(a) 12S-CH *(c) 12S-SD*

(b) 3S-CH *(d) 3S-SD*

Fig. 8. MCE-level peak BRB normalized axial forces, P_u/P_{ye} (mean of maximums).

the estimated response Est. (E+G) is compared with the NLRHA response because both represent forces induced by combined seismic and gravity effects. The comparison between Est. (E+G) and Est. (E) demonstrates how gravity affects the member forces. In the axial force diagrams, only Est. (E) is presented for comparison with the NLRHA response, since the axial forces are due to the seismic effect alone. Notably, across all three design cases (Figure 9), the strong agreement between the Est. (E+G) and NLRHA responses in the shear and moment diagrams, along with the fair match between Est. (E) and the NLRHA axial force diagrams, validates the proposed analysis methods for estimating beam force demands in the capacity design of chevron BRBFs.

For concentric Case 12S-CH-C [Figure 9(a)], the Est. (E+G) and NLRHA curves in the shear and moment diagrams show low shear and moment demands in the concentric chevron BRBF beams. In the moment diagram, the Est. (E) curve reveals a certain amount of negative bending moment induced by the seismic effect, which arises from the net upward brace force due to the imbalance between the two brace forces beneath the beam. Meanwhile, the low magnitude of the Est. (E+G) response suggests that gravity effect helps counteract the seismic-induced moment.

For Cases 12S-CH-E1d [Figure 9(b)] and 12S-CH-E2d [Figure 9(c)], significant shear and moment demands are induced in the beams due to brace eccentricity. Comparing the shear diagrams between these two eccentric frames reveals a trend: As brace eccentricity increases, the shear demand in the interior region slightly decreases, while there is a moderate increase in shear demands in the exterior regions. This shift highlights the impact of increasing eccentricity on the distribution of shear forces along the beam.

The comparison of moment diagrams between the two eccentric design cases [Figures 9(b) versus 9(c)] reveals

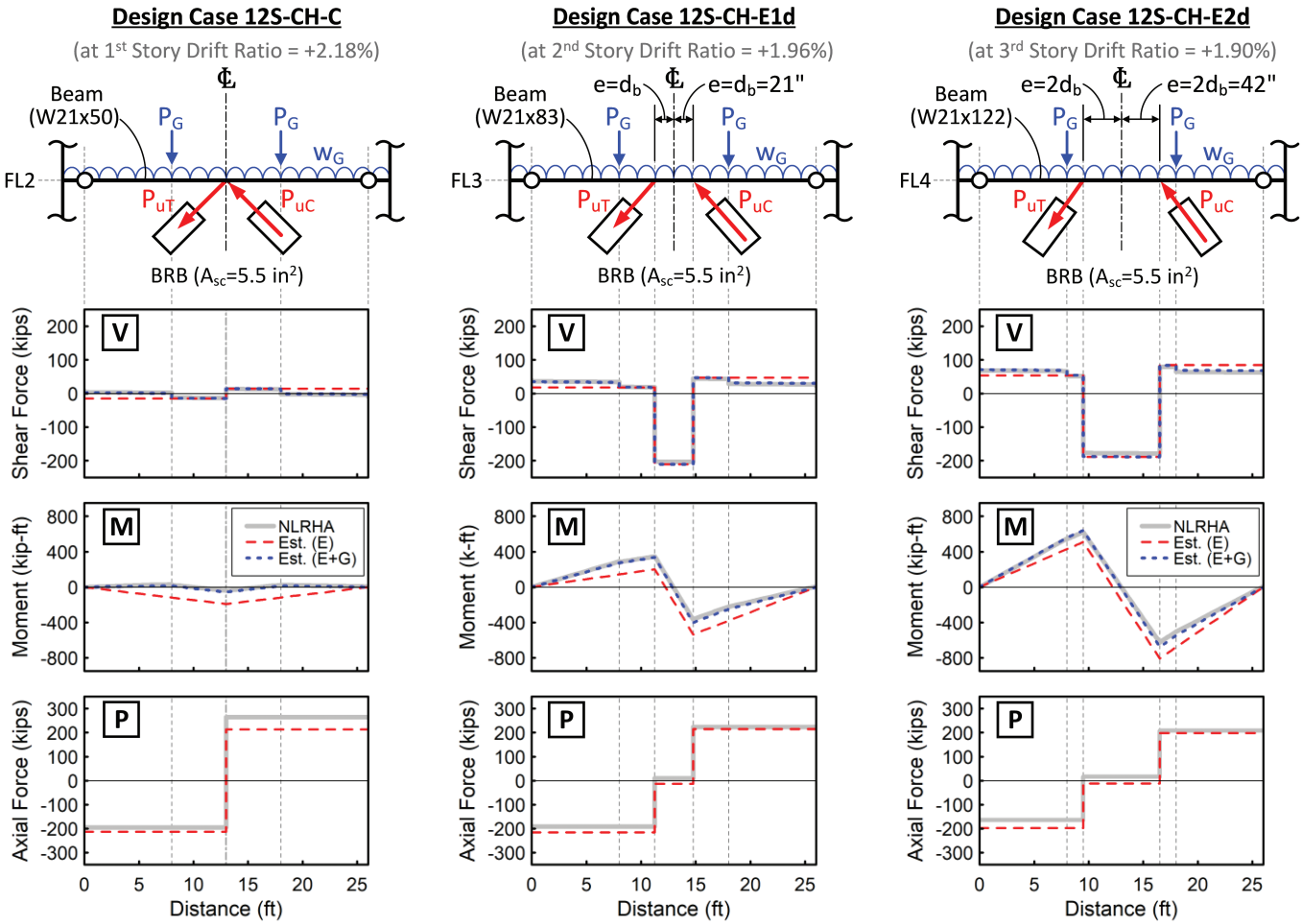

(a) 12S-CH-C, floor 2 *(b) 12S-CH-E1d, floor 3* *(c) 12S-CH-E2d, floor 4*

Fig. 9. Member forces in selected beams from a NLRHA.

a clear trend: The beam moment demand increases with brace eccentricity. Noticeable discrepancies between the Est. (E+G) and Est. (E) moment diagrams are seen in both eccentric frames. The seismic-induced moment diagram [Est. (E)] shows a notable imbalance in the magnitude of moment demands between the two exterior beam regions, stemming from the imbalance between the brace forces. In contrast, this imbalance is insignificant in the total action diagram [Est. (E+G)], indicating that the gravity effect tends to offset the discrepancies in moment demand between the two exterior regions.

In the beam axial force diagrams (Figure 9-bottom), comparing the three cases shows a similarity in the magnitude of the peak axial forces. It can be observed that the axial force magnitude slightly decreases with increasing eccentricity, primarily due to the steeper brace angle, which results in a reduced horizontal component of the brace forces.

In summary, for chevron BRBF beams with eccentricities [Figures 9(b) and 9(c)], the interior beam region experiences higher shear forces and relatively lower axial forces, while the exterior beam regions are subject to significant *P-M* interaction demands. When the brace eccentricity is small, the shear design of the interior region may dominate beam sizing. However, as eccentricity increases, the beam sizing is likely to be governed by the *P-M* interaction in the exterior regions.

Figure 10 shows selected beam force diagrams from the 12-story single-diagonal BRBF design cases. Beams on the 4th and 3rd floors were selected for Cases 12S-SD-C and 12S-SD-E2d, respectively, as braces beneath both beams are identical in size (A_{sc} = 8.0 in.^{2}). The forces are shown at point in time when the story below each beam reached about 0.02 rad drift. The NLRHA responses are plotted alongside the estimated force diagrams calculated using the proposed analysis methods. Curves labeled Est. (E), Est. (G), and Est. (E+G) represent the estimated force diagrams for the seismic effect only, gravity effect only, and combination of two effects, respectively. Overall, Figure 10 demonstrates good agreement between the NLRHA and estimated responses across all force diagrams, validating the accuracy of the proposed analysis methods in estimating beam force demands for the capacity design of single-diagonal BRBFs.

As described in Part 1 (Li et al., 2026), the asymmetry of the frame geometry requires two analysis cases for the capacity design of single-diagonal BRBFs. Analysis Case 1 refers to the scenario where seismic loading causes tension in the braces, while Analysis Case 2 involves seismic loading causing compression in the braces. For the concentric Case 12S-SD-C [Figure 10(a)], only the beam actions at positive story drift (braces in tension) are shown since Analysis Case 1 governs the beam capacity design in the concentric frame, as further explained in the following paragraph. In contrast, for the eccentric Case 12S-SD-E2d, beam actions at both positive [Figure 10(b)] and negative [Figure 10(c)] drifts—corresponding to Analysis Cases 1 and 2, respectively—are presented to account for both design scenarios.

In the concentric Case 12S-SD-C [Figure 10(a)], the beam shear and moment demands are primarily due to the gravity effect, as shown by the close alignment of the NLRHA and Est. (G) force diagrams. Thus, these demands remain unchanged regardless of the frame drift direction. For beam axial force [Figure 10(a)-bottom], the compressive force occurs when the braces above and below the beams are in tension, corresponding to Analysis Case 1 for capacity design. Note that the ultimate compressive force in the beam is driven by the maximum possible tensile brace forces, estimated by the tensile adjusted brace strength, P_{uT}, while the ultimate tensile beam force corresponds to the compressive adjusted brace strength, P_{uC}. Since P_{uC} is about 10% higher than P_{uT} (i.e., $\beta = 1.1$) for the braces used for this design case, the magnitude of the ultimate tensile force is expected to exceed the compressive force by around 10%. However, the compressive beam force scenario (Analysis Case 1) is considered to govern the beam design, as a beam's compressive strength is typically lower than its tensile strength by more than 10%.

For the eccentric Case 12S-SD-E2d [Figures 10(b) and 10(c)], each level's BRBF beam consists of two members: the stub and the beam. The shear and moment diagrams indicate that the stub, acting as a cantilever beam, carries significant shear and moment, while the beam member experiences relatively low magnitudes of both demands. Notably, in the shear and moment diagrams within beam member range, the approximately zero magnitude of the Est. (E) curves and the close alignment of the NLRHA and Est. (E+G) responses indicate the two demands in the beam are primarily due to the gravity effect.

In addition, the peak values of shear and moment demands [Figures 10(b) and 10(c)] on the beam member in the eccentric frame are slightly lower than those in the concentric frame [Figure 10(a)], likely due to the shorter length of the beam member in the eccentric frame. This suggests that potentially lighter beam members could be used in the eccentric frame.

For the axial actions in the beam member, it carries high magnitudes of compressive force [Figure 10(b)-bottom] when the adjacent brace is in tension (Analysis Case 1) and axial tension [Figure 10(c)-bottom] when the brace is in compression (Analysis Case 2). Thus, Analysis Case 1 governs the beam member design, as it has a lower capacity in compression.

Regarding the stub, the shear and moment diagrams corresponding to positive drift (braces in tension) [Figure 10(b)] show higher magnitudes for the NLRHA and Est.

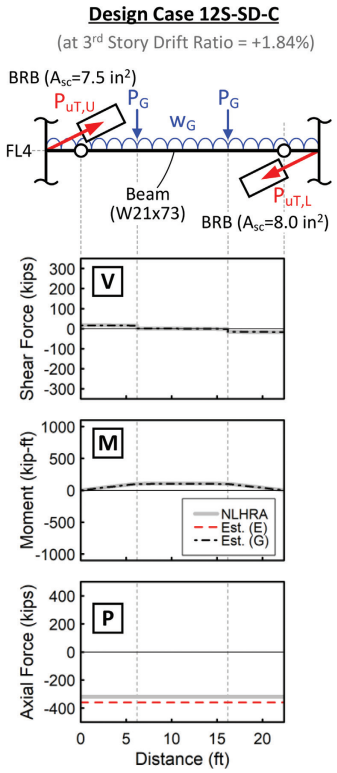

(a) 12S-SD-C, floor 4 at positive drift

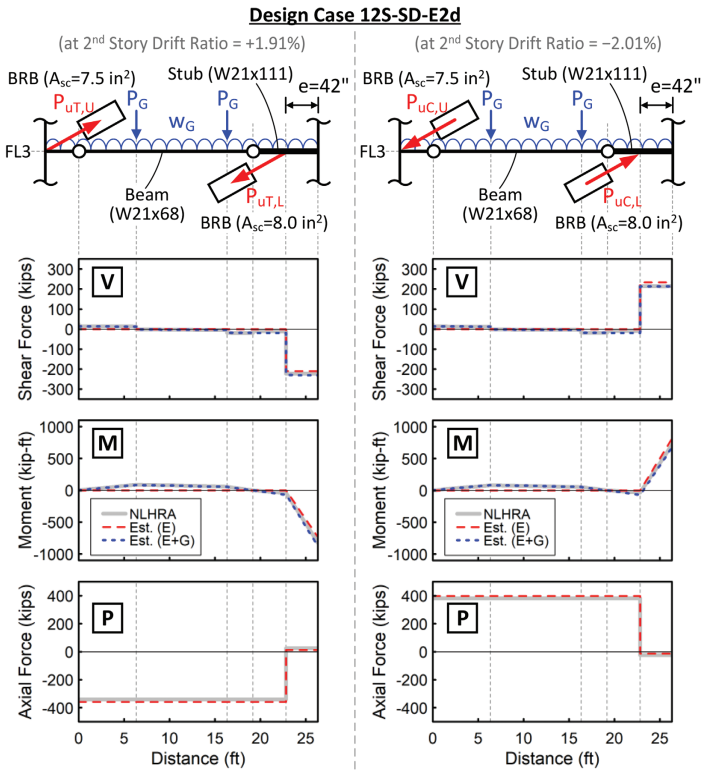

(b) 12S-SD-E2d, floor 3 at positive drift

(c) 12S-SD-E2d, floor 3 at negative drift

Fig. 10. Member forces in selected beams from a NLRHA.

(E+G) responses compared to the Est. (E) response, indicating that the seismic and gravity effects are additive in Analysis Case 1. Conversely, when the adjacent brace is in compression [Figure 10(c)], the magnitudes of NLRHA and Est. (E+G) responses for shear and moment in the stub are lower than those of the Est. (E) response, suggesting that the gravity effect counteracts the seismic effect in Analysis Case 2.

Although the seismic effect is the primary source of the shear and moment demands in the stub, and the magnitudes of seismic-induced demands [Est. (E) response] are expected to be higher in Analysis Case 2 (braces in compression) due to $P_{uC} > P_{uT}$, the total shear and moment demands under the combined seismic and gravity effects in Analysis Case 1—where the two effects are additive—may be higher than the total demands in Analysis Case 2, evidenced by the selected beam responses shown in Figures 10(b) and 10(c). On the other hand, when the adjacent brace has a high β value (i.e., high compression overstrength), the stub may experience higher total shear and moment demands in the Analysis Case 2.

For the axial actions in the stub, it experiences low magnitudes of axial tension [Figure 10(b)-bottom] when the adjacent brace is in tension (Analysis Case 1) and compression [Figure 10(c)-bottom] when the brace is in compression (Analysis Case 2). Although Analysis Case 2 is more critical for the stub's axial action due to being in compression and having a lower capacity, there remains a possibility that the high shear and moment demand in Analysis Case 1 could govern the design. In summary, both Analysis Cases 1 and 2 must be considered for the capacity design of subs.

Column Axial Response

Figure 11 shows the compressive axial demand-to-capacity ratios (DCRs), $P_u/(\phi P_n)$, for the BRBF columns obtained from the NLRHA. Here, P_u is the mean peak compressive forces, averaged from 16 ground motions, for the columns in each story, and ϕP_n is the design compressive strength calculated in accordance with the AISC *Specification for Structural Steel Buildings* (2022b). For the chevron BRBFs, where identical member sizes are used for both sides of columns due to the symmetry of the structure, P_u is taken as

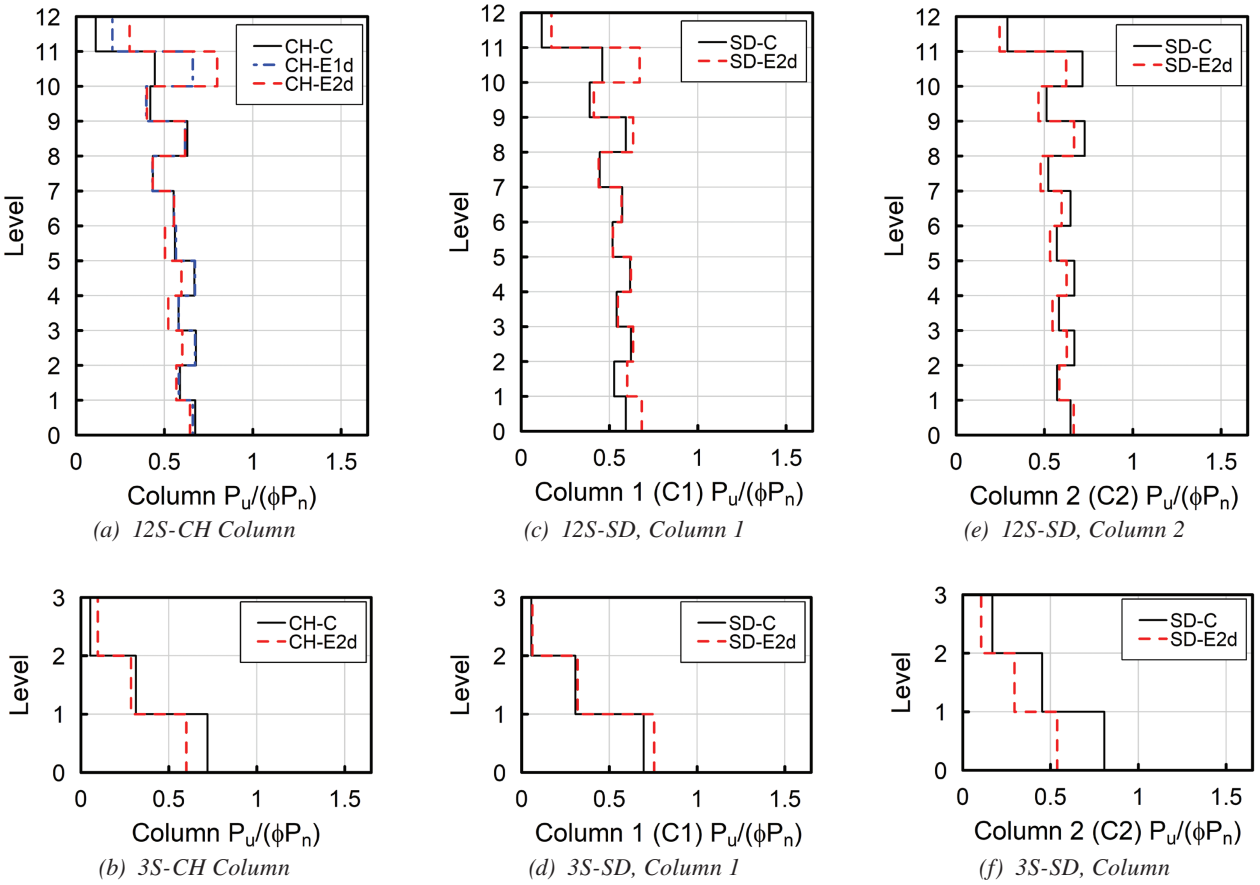

(a) 12S-CH Column (c) 12S-SD, Column 1 (e) 12S-SD, Column 2

(b) 3S-CH Column (d) 3S-SD, Column 1 (f) 3S-SD, Column

Fig. 11. MCE-level compressive DCRs, $P_u/(\phi P_n)$ (mean of maximums).

the larger of peak responses between the two columns in the same story. In contrast, for the single-diagonal BRBFs, where the structure is asymmetric, the columns on each side are designed separately. As illustrated in Figures 1(c) and 1(d), the Column 1 (C1) members refers to the side of the columns adjacent to the brace bottom ends (away from the stubs in eccentric frames), while Column 2 (C2) members refers to the columns adjacent to the brace top ends (next to the stubs in eccentric frames). For these single-diagonal frames, the compressive DCRs for C1 and C2 members were determined separately and are presented individually in Figure 11.

Overall, Figure 11 shows that the column compressive DCR distributions along the building height are similar between the concentric and eccentric BRBFs for all groups, except for Column 2 in Group 3S-SD [Figure 11(f)], where the DCRs of C2 members in Case 3S-SD-E2d were notably smaller than those in 3S-SD-C throughout the building height. This is due to the C2 member size in 3S-SD-E2d being increased to meet the compactness requirements for moderately ductile members, resulting in oversized columns for capacity design. This is reflected in the low DCR values (e.g., 0.62 for the first-story C2 member) in capacity design check as shown in Table 11 of Part 1 (Li et al., 2026). For the 12-story design cases [Figures 11(a), 11(c), and 11(e)], most of the column compressive DCRs from NLRHA ranged between 0.5 to 0.7. For the 3-story frames [Figures 11(b), 11(d), and 11(f)], the largest NLRHA column DCRs, occurring in the first story in each frame, reached about 0.6 to 0.8. It is worth noting that most first-story columns were sized based on the demand from capacity design, with no oversizing for conservatism, as indicated by the capacity design DCR values for exceeding 0.95 [see Tables 10 and 11 of Part 1 (Li et al., 2026)]. As a result, the column design strength ϕP_n closely matches the estimated demand in capacity design, making the NLRHA column DCRs in the first story reflect the ratio of peak dynamic response to the expected axial demand. Thus, the first-story column DCRs in Figure 11 can serve as an index for evaluating the conservatism of the capacity design. The DCR values being notably lower than 1.0 suggest that the assumed plastic mechanism used in capacity design—where all braces in a BRBF develop the adjusted brace strengths (P_{uT} or P_{uC})—is somewhat conservative for estimating the column axial demand, also indicating a low likelihood of simultaneous yielding (to reach the adjustment braces strength) of all braces in a BRBF during the earthquakes.

DETAILED FINITE ELEMENT ANALYSIS

To complement the response history analysis, additional simulations were performed to investigate the stress state in BRBF beams when braces reach design deformations. Pushover analyses were performed on individual frame models where the geometry of the beam and gussets in the connection region were considered explicitly. The ANSYS software (ANSYS, 2022) was used for these analyses.

Frame Geometries

Figure 12 illustrates three frames that were investigated: BRBF-CH-C, BRBF-CH-E1d, and BRBF-CH-E2d. The beam, column, and brace sizes for the frames, came from the first-story designs of the 12-story chevron case study frames: 12S-CH-C, 12S-CH-E1d, and 12S-CH-E2d, respectively. [See Table 1 of Part 1 (Li et al., 2026) for the member sizes.] The three frames have comparable design strength, but different brace and beam sizes based on the proposed design procedures for BRBF with eccentricity (see Section 2 of Part 1).

Modeling Techniques

Three types of elements were used in the models to represent the various components efficiently. The gusset and beam (in the connection region) were modeled with solid hexahedral elements (SOLID186), with a 1 in. mesh size. The gusset-to-beam welds were not modeled explicitly. Outside the gusset region, the beam was represented with elastic beam elements (BEAM188), as were the columns. The BRBs were represented with nonlinear springs

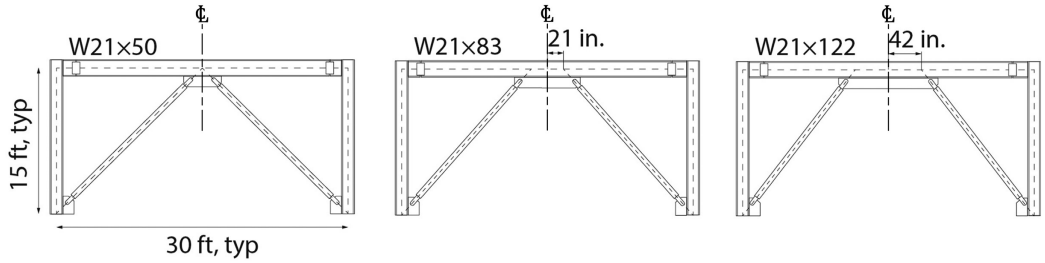

(a) BRBF-CH-C *(b) BRBF-CH-E1d* *(c) BRBF-CH-E2d*

Fig. 12. Frame geometries investigated with detailed finite element analysis.

(COMBIN39) with the elastic stiffness, yield strength, and the post-yield properties summarized in Table 4 of Part 1 (Li et al., 2026).

The boundary conditions and loading in the model were for a displacement-controlled pushover analysis (Figure 13). The column bottom nodes were pinned. Fully restrained connections were assumed at the beam-to-column connection, reflecting gusset plates that would be present from the story above (not modeled). Brace connections were modeled as pinned at each end. The frame was constrained against any out-of-plane displacements. For the lateral loading, in-plane horizontal displacements were imposed at the nodes at the top of the columns. The displacements were ramped up to 3.6 in., corresponding to 2% story drift.

The materials in the finite element (FE) model, for the beams, columns, and gussets, simulated nominal steel properties (Grade 50 material). The elastic modulus was 29,000 ksi, Poisson's ratio was 0.3, yield stress was 50 ksi, and the post-yield modulus was 150 ksi (the material would reach the nominal tensile strength of 65 ksi at 0.1 strain). The material models, with nominal strengths, were appropriate for checking the presence of undesirable yielding/deformations in the beams and gussets.

Validation

As a check on the reasonableness of the models, the results from the pushover analyses were compared with pushover results from centerline models, with the same modeling techniques as used for the NLRHA (discussed earlier). Brace force-deformation plots were checked to confirm that the braces were represented as shown in Figure 2(b).

Figure 14(a) shows the pushover curves for the solid-element models (solid), and the reference centerline models (dashed). For all three geometries, the solid-element model, where the connection geometry was explicitly represented, had essentially the same pushover curve as the centerline model. The frames with eccentricity had less elastic stiffness than the concentric frame, as was previously discussed, but all the frames had similar lateral strength and post-yield stiffness (governed by the braces).

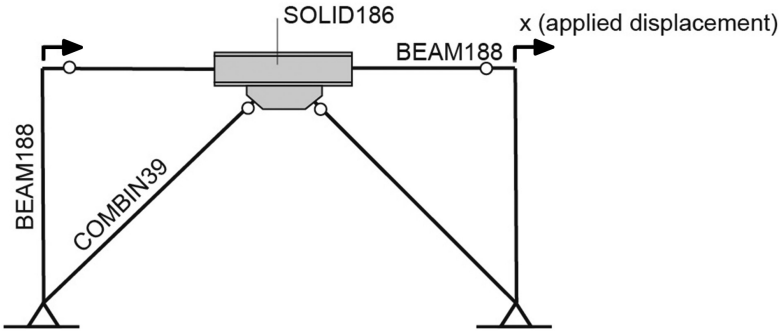

Fig. 13. Element types and boundary conditions for the FE analysis.

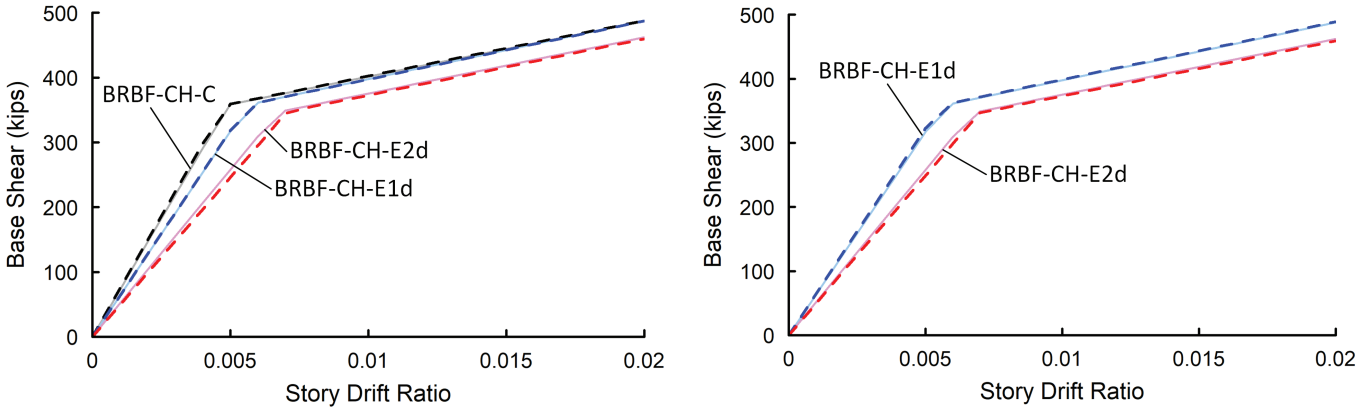

(a) Single gusset models (solid line) and centerline models (dashed line)

(b) Single gusset models (solid line) and split gusset models (dashed line)

Fig. 14. Pushover curves from the detailed FE analysis.

Results

Figure 15 shows the displaced geometry and the equivalent (von Mises) stress in the connection region for the frames at 2% story drift. From Figure 15, beam deformations are essentially imperceptible at that drift. Figure 15(a) shows the case for BRBF-CH-C with a W21×50 beam. The colored contours show that the equivalent (von Mises) stress reached 39.0 ksi in the center of the beam web, caused by beam shears from the chevron effect (Sabelli and Arber, 2017), which was considered in design. Figure 15(b) shows BRBF-CH-E1d (W21×83 beam), where the equivalent (von Mises) stress reached 35.3 ksi in the center of the beam web, caused by beam shears from the eccentricity (which were considered in the design). The design procedure for the beam conservatively neglected any shear carried by the gusset plate. The model confirmed that the design methods discussed in the second section of Part 1 (Li et al., 2026) are conservative for preventing the beam from reaching a shear yielding limit state, even when the braces are at their design deformation. Figure 15(c) shows BRBF-CH-E2d (W21×122 beam), where the web stresses reflect beam shears and moments caused by the eccentricity. Here, the equivalent (von Mises) stress was even further below 50 ksi, at 29.6 ksi in the center of the beam web, confirming the reasonableness of the design approach. Considering all three together,

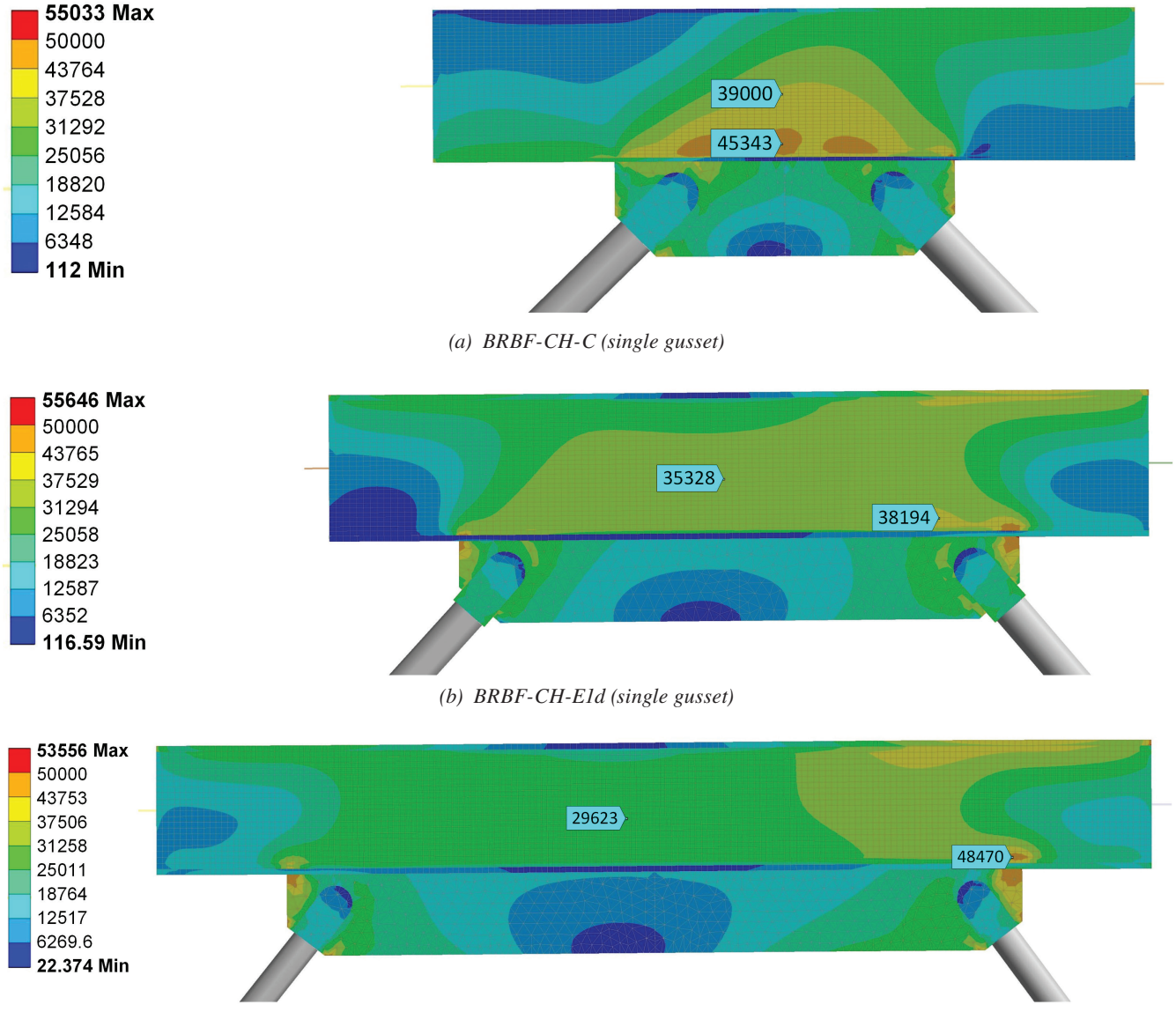

(a) BRBF-CH-C (single gusset)

(b) BRBF-CH-E1d (single gusset)

(c) BRBF-CH-E2d (single gusset)

Fig. 15. Equivalent (von Mises) stress contours (unit: psi) in the gusset connection regions at 2% story drift in single gusset models.

BRBF-CH-E1d and BRBF-CH-E2d had lower shear stress in the beam web than BRBF-CH-C, and the source of the beam web shear stress was different (the chevron effect for BRBF-CH-C, and connection eccentricity for BRBF-CH-E1d and BRBF-CH-E2d).

Figures 16 and 14(b) shows results for variants of the models that have split gusset plates. From Figure 16, the split gusset plate results in higher beam web stresses, but a limit state has not been reached. The two cases in Figure 16 appear to be on the verge of requiring stiffeners to address web local yielding in the beam at the end of the gusset. From Figure 14(b), the pushover curves are essentially the same for the combined (i.e., single) and split gusset configuration. For the BRBF-CH-E1d frame, the combined gusset model exhibits slightly less elastic lateral stiffness compared to the split gusset model, which was unexpected and is likely due to the increased flexural deformations in the beams outside the combined gusset. However, for the BRBF-CH-E2d frame, the combined gusset slightly enhances the frame's elastic lateral stiffness compared to the split gusset.

Moreover, the stress ratios of the equivalent stress in the beam web (within the eccentricity range) divided by the yield stress of 50 ksi, as obtained from the split-gusset models (Figure 16), are approximately 0.88 and 0.74 for BRB-CH-E1d and BRB-CH-E2d, respectively. For comparison, an adjusted DCR for PV interaction, denoted as $DCR_{PV,adj}$, is introduced. This value is obtained by multiplying the estimated DCR_{PV} of chevron beam design [listed in Table 8 in Part 1 (Li et al., 2026)] by ϕ_v to remove the conservatism inherent in the ϕ_v factor. The calculated $DCR_{PV,adj}$ values for the first-story beams in Design Cases 12S-CH-E1d and 12S-CH-E2d are about 0.86 and 0.73, respectively, both of which are close to the beam web stress ratios developed in the corresponding FE model. It should be noted that the estimated DCR_{PV} was based on the simplified beam model using concentrated brace forces without considering the local chevron effect (Fortney and Thornton, 2017) from the chevron gusset connection geometry. The strong agreement between $DCR_{PV,adj}$ values and stress ratios from FE models reflecting the localized effect indicates that the chevron effect is small relative to the shears and moments caused by the eccentricity.

DESIGN IMPLICATIONS ON SINGLE-DIAGONAL BRBF WITH ECCENTRICITY

Design of Half-Moment Frame Column

General

When a single-diagonal BRBF with eccentricity is subjected to lateral forces, as illustrated in Figure 17, the stubs transfer bending moments to the adjacent Column 2 (C2) members due to the moment connections between the stubs

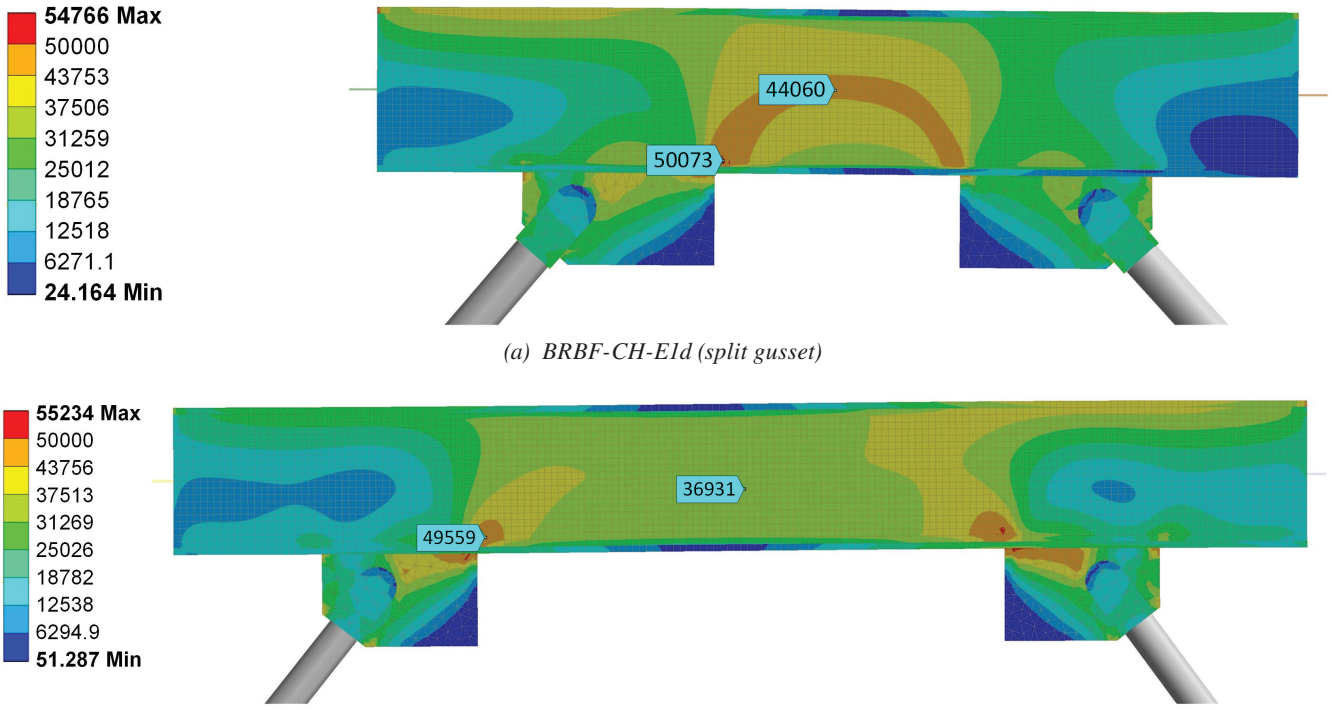

(a) BRBF-CH-E1d (split gusset)

(b) BRBF-CH-E2d (split gusset)

Fig. 16. Equivalent (von Mises) stress contours (unit: psi) in the gusset connection regions at 2% story drift in split gusset models.

and C2 members that make up the half-moment frames. This moment demand can become significant, especially in cases where the eccentricity is large. Although the AISC *Seismic Provisions* (2022a) permit the neglecting of seismic-induced moment demands in the design of conventional BRBF columns, it is unclear whether this provision is suitable for single-diagonal eccentric BRBFs. Therefore, this sub-study examines the impact of including moment demands in the design of C2 members through a series of NLRHA analyses, which will be discussed in this section.

Estimation of Moment Demand in Column

This study proposes a method, illustrated in Figure 17, to estimate seismic moment demands in the C2 members. Recall that two analysis cases must be considered separately for capacity design of single-diagonal BRBFs. Analysis Cases 1 and 2 refer to the scenarios where seismic loading causes the braces in tension and compression, respectively. Figures 12 and 13 of Part 1 (Li et al., 2026) present the axial force analyses in column capacity design for these respective analysis cases. It is hypothesized that the governing moment demand in C2 members would occur in Analysis Case 1, rather than Analysis Case 2, for two reasons:

1. Axial load interaction: In Analysis Case 1, as shown in Figure 12 of Part 1, C2 members are subjected to overturning (OT) compression, and simultaneous moment demands should be considered for the combined axial-flexure (*P-M*) interaction design. This makes Analysis Case 1 more critical as the interaction between axial compression and bending moments intensifies the demand on C2 members.
2. Combination of seismic and gravity effects: In Analysis Case 1, as shown in Figure 9 of Part 1, seismic and gravity effects on the bending actions in the stubs are additive. In contrast, these two effects counteract each other in Analysis Case 2, as depicted in Figure 10 of Part 1. Consequently, both the stubs and the adjacent C2 members are expected to resist higher moment demands in Analysis Case 1 compared to Analysis Case 2 under typical conditions. An exception to this could occur if the brace exhibits high compression overstrength, indicated by a high β value, which could lead to higher moment demands in the stub and C2 members in Analysis Case 2. Despite this, Analysis Case 1 would still govern the design because C2 members experience OT tension in Analysis Case 2, which is less critical than OT compression in Analysis Case 1.

The proposed distribution of seismic moments at stub-to-column intersections is illustrated in Figure 17-right. This approach estimates the capacity-limited seismic load effects, E_{cl}, on C2 member end moments. First, the maximum moment at the stub is determined in Analysis Case 1, where each stub is subjected to the tensile adjusted strength, P_{uT}, from the adjacent brace. The seismic moment at the ith level stub's end, $M_{Ecl1,Stub,i}$ (where the subscript $Ecl1$ refers to E_{cl} effect in Analysis Case 1), is given by:

$$M_{Ecl1,Stub,i} = e(P_{uT,i}\sin\theta_i) \tag{1}$$

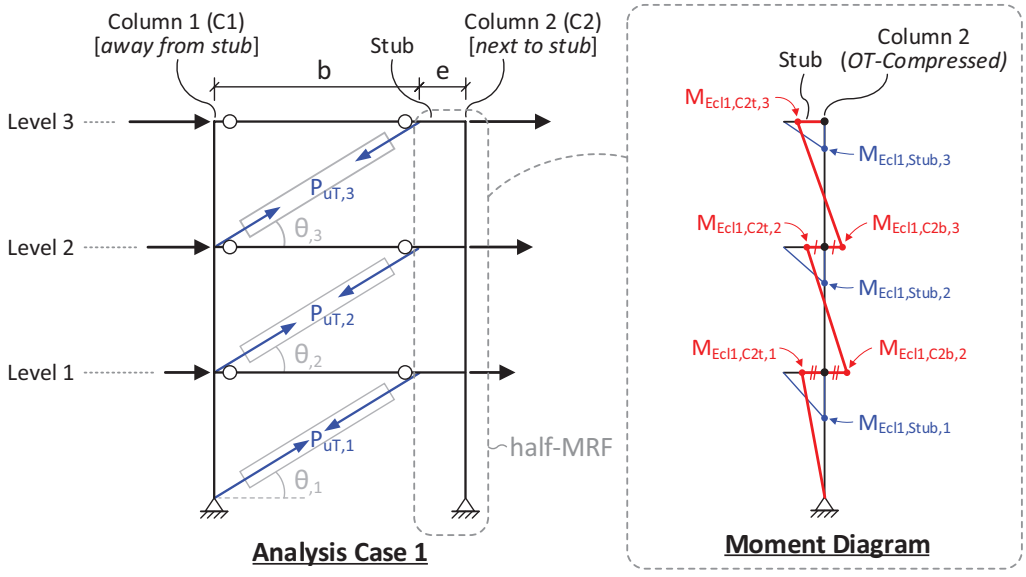

Fig. 17. Estimation of capacity-limited seismic load effects on moment demands in Column 2 (C2) members in a single-diagonal eccentric BRBF.

Here, $P_{uT,i}$ is the tensile adjusted strength, and θ_i is the inclination angle of the ith story brace.

For typical floors, the seismic moment at the stub end calculated from Equation 1 is assumed to be equally distributed between the adjacent C2 members above and below the stub:

$$M_{Ecl1,C2b,i+1} = M_{Ecl1,C2t,i} = \frac{M_{Ecl1,Stub,i}}{2} \tag{2}$$

At the roof (Nth level), the entire stub-end moment is transferred to the adjacent C2 member's top end:

$$M_{Ecl1,C2t,N} = M_{Ecl1,Stub,N} \tag{3}$$

Finally, the total moment demand at the ends of C2 member, $M_{u,C2}$ for beam-column design is determined by combining gravity and seismic load effects:

$$M_{u,C2} = B_1\left[(1.2+0.2S_{DS})M_{D,C2} + f_L M_{L,C2}\right] + M_{Ecl1,C2} \tag{4}$$

where $M_{D,C2}$ and $M_{L,C2}$ are the moments due to dead and live loads, respectively; f_L is the load factor for live load; $M_{Ecl1,C2}$ is the capacity-limited seismic moment estimated from Equations 2 or 3; S_{DS} is the design spectral response acceleration parameter at short periods (ASCE, 2022); and B_1 is the multiplier factor from AISC *Specification* Appendix 8 (AISC, 2022b), accounting for the P-δ effect.

It is important to acknowledge that the assumption of equal moment distribution between the columns may underestimate the peak dynamic moment at one of the columns at the stub-to-column intersection during seismic events. The actual distribution of moments may be influenced by the relative flexural stiffness of the two adjacent columns and higher-mode effects of the building. Consequently, the distribution may not be perfectly symmetrical, especially when stiffness variations or higher-mode effects are significant. Nonetheless, the assumption of even moment distribution offers a practical simplification for design purposes. Additionally, as shown in Figure 11, the capacity design method often overestimates the actual peak axial force in the columns during earthquakes, indicating some tolerance for underestimating moment demand in combined axial and flexural design. A series of NLRHA were conducted, and the results of these analyses will be presented later to provide further insight into the adequacy of the proposed column moment demand estimations.

Candidate Design Methods and Additional Design Cases

To investigate the effect of including moment demand for design of C2 members, three candidate design methods were utilized in this study for sizing and resizing the C2 members in Design Cases 12S-SD-E2d and 3S-SD-E2d. The three design methods are described as follows:

1. Design Method N (axial-only design): The designation N refers to normal and axial-only design, where the C2 members in the single-diagonal eccentric BRBFs are treated as the normal BRBF columns. The seismic moment is neglected, as permitted by the AISC *Seismic Provisions* (2022a), provided the capacity-limited seismic effect is considered for sizing the BRBF columns. Further, in the design cases considered in this study, the gravity moment demands in the C2 members are minimal and considered negligible. Therefore, for Design Method N, the C2 members are designed based solely on axial force demand, excluding moment demand from the design process. The demand-to-capacity ratio (DCR) for axial force, DCR_P, is calculated as:

$$DCR_P = \frac{P_u}{\phi_c P_n} \tag{5}$$

where P_u is the axial force due to combined gravity and capacity-limited seismic effects [as determined in Part 1, Equations 24 and 26 (Li et al., 2026)], and $\phi_c P_n$ is the design compressive strength.

2. Design Method M (strong column–weak beam design): The label M stands for moment-resisting frame (MRF) column design. This method acknowledges that the stubs and C2 members in a single-diagonal eccentric BRBF function together as a half-MRF [Figures 1(c) and 1(d)] and thus treats the C2 members as MRF columns. The strong column–weak beam (SCWB) design approach, which is typically used for the special moment frame (SMF) columns, is adapted for sizing the C2 members. The associated DCR, DCR_{SCWB}, for each stub-to-column intersection is calculated as:

$$DCR_{SCWB} = \frac{M_{u,Stub}}{\sum M^*_{pc}} = \frac{M_{u,Stub}}{\sum\left[Z_{xc}\left(F_{yc} - \frac{P_u}{A_{gc}}\right)\right]} \tag{6}$$

The term $M_{u,Stub}$ is the total stub-end moment demand projected to column centerlines, incorporating both gravity effect and capacity-limited seismic effect from the adjacent brace's adjusted strength. This differs from the conventional SCWB equation for SMF, which uses the sum of beam plastic moment projections to the column centerline, as shown in ΣM^*_{be} in the AISC *Seismic Provisions* (2022a), reflecting the different performance objectives between the half-MRF and SMF.

It is also noted that the stubs and moment connections between the stubs and C2 members are designed to remain elastic, with force demands capped by the adjacent braces' capacity. Therefore, the stub-to-column connections do not require strict seismic detailing typical of SMFs, such as WUF-W welds. Additionally, these

welds can be made in the shop, with quality achieved without seismic detailing. The equation for determining $M_{u,Stub}$ is as follows:

$$M_{u,Stub} = (1.2 + 0.2S_{DS})M_{D,Stub} + f_L M_{L,Stub} + M_{Ecl1,Stub} \quad (7)$$

where $M_{D,Stub}$ and $M_{L,Stub}$ are the moments due to dead and live loads, respectively, and $M_{Ecl1,Stub}$ is the capacity-limited seismic moment, estimated from Equation 1. The term ΣM^*_{pc} in Equation 6 is the sum of the nominal flexural strengths of the columns above and below the stub-to-column intersection, projected to the beam centerline, with a reduction for the total axial demand, P_u, including seismic capacity-limited effect in C2 members, as determined in Part 1, Equations 24 and 26 (Li et al., 2026). The symbols F_{yc}, A_{gc}, and Z_{xc} in Equation 6 denote the nominal yield strength, gross area, and plastic modulus, respectively, for the C2 member. Notably, in contrast to the SCWB equation for SMF, the column capacity term ΣM^*_{pc} is intentionally placed in the denominator term of Equation 6 to ensure that a value of $DCR_{SCWB} \leq 1.0$ indicates compliance of SCWB requirements. This arrangement facilitates discussions concerning two other candidate design methods.

3. Design Method X (*P-M* interaction design): The notation X signifies the extra conservatism in the *P-M* interaction design check for C2 members, with an attempt to maintain their elasticity under the capacity-limited seismic effect for both axial and flexural demands. In this design method, the associated DCR, DCR_{PM}, is calculated using the *P-M* interaction equation in AISC *Specification* Chapter H (2022b) as follows:

$$DCR_{PM} = \begin{cases} \left|\frac{P_u}{\phi P_n}\right| + \frac{8}{9}\left|\frac{M_u}{\phi_b M_n}\right|, \ for \left|\frac{P_u}{\phi P_n}\right| \geq 0.2 \\ \frac{1}{2}\left|\frac{P_u}{\phi P_n}\right| + \left|\frac{M_u}{\phi_b M_n}\right|, \ for \left|\frac{P_u}{\phi P_n}\right| < 0.2 \end{cases} \quad (8)$$

where P_u [Part 1, Equations 24 and 26 (Li et al., 2026)] and M_u (Equation 4) represent total axial and flexural demands, respectively, including the capacity-limited seismic effect. In Equation 8, the design axial strength ϕP_n is taken as the compressive strength $\phi_c P_n$, and $\phi_b M_n$ is the design flexural strength.

It is worth noting the comparison of the design intentions of the three methods (N, M, and X). First, Design Method N follows the general rule from the AISC *Seismic Provisions* (2022a) for designing columns in the seismic force resisting system (SFRS), where the SFRS columns are designed based solely on axial force demand (i.e., Design Method N), provided the capacity-limited seismic effect is included in the axial force calculation. This approach aims to prevent global column failure but does not guarantee the columns from yielding under the combined axial and moment demands. The rationale is that in the SFRS, bending moments tend to peak at the column ends, often resulting in reversed curvature in the columns, which minimizes the impact of bending moments on column buckling. With this relaxation in ignoring moment demand, Design Method N serves as the "baseline" for C2 member design.

Second, Design Method M adopts the strong column–weak beam (SCWB) design concept, which is specific to SMF systems, to address the potential issue of the significant moments in the MRF columns. This approach aims to ensure that columns are strong enough to avoid concentrating inelastic action in a single story, though it offers no assurance that individual columns will remain elastic. Notably, the SCWB method evaluates the reduced moment capacity due to axial force using the sectional yield criterion, without considering column buckling, making it less stringent in estimating the moment strength than the typical *P-M* interaction check for beam-column design. In summary, the SCWB-based Design Method M represents the code-specified additional design criterion for SMF columns, typically subjected to significant moments. In SMF column design, the SCWB method often surpasses the axial-only approach, which is the baseline design for general SFRS columns, and governs the final design, particularly in moment-critical scenarios.

Lastly, Design Method X incorporates the proposed estimation of column moment demand into *P-M* interaction check for conducting beam-column design of C2 members. This method aims to maintain elasticity of C2 members under combined axial and flexural forces, including capacity-limited seismic effects. It is stricter than the AISC *Seismic Provisions* (2022a) requirements for columns in any SFRS system and typically results in a heavier design than the other two methods. Thus, Design Method X embodies extra conservatism beyond regulatory standards. Despite this conservatism, its effectiveness in preventing the yielding of individual columns is evaluated through the NLRHA studies presented later.

Note that the C2 members in both single-diagonal eccentric cases, 12S-SD-E2d and 3S-SD-E2d, presented earlier were effectively sized using Design Method N. In addition to the two original cases, the C2 members in these two designs were redesigned using Design Methods M and X, while keeping the sizes of the other members (braces, beams, and C1 members) the same. This resulted in three additional design cases, bringing the total to five design cases of single-diagonal eccentric BRBFs, which will be discussed later. Tables 3 and 4 summarize the design results of the C2 members, including member sizes and associated DCRs for the three design methods across the five design

Table 3. Design DCRs for Column 2 (C2) in Two Designs of 12-Story Single-Diagonal Eccentric BRBFs								
	12S-SD-E2d-N/M (= Original 12S-SD-E2d)				12S-SD-E2d-X			
Story	C2 Shape	DCR_P	DCR_{SCWB}	DCR_{PM}	C2 Shape	DCR_P	DCR_{SCWB}	DCR_{PM}
12	W14×48	0.33	0.96	1.13	W14×68	0.18	0.62	0.70
11	W14×48	0.86	0.95	1.62	W14×68	0.47	0.58	0.98
10	W14×82	0.65	0.92	1.11	W14×109	0.39	0.55	0.73
9	W14×82	0.93	0.91	1.43	W14×109	0.56	0.53	0.93
8	W14×120	0.67	0.87	1.03	W14×145	0.54	0.55	0.84
7	W14×120	0.84	0.86	1.23	W14×145	0.68	0.57	1.00
6	W14×159	0.76	0.86	1.07	W14×193	0.62	0.55	0.87
5	W14×159	0.91	0.88	1.24	W14×193	0.74	0.54	1.01
4	W14×211	0.79	0.82	1.05	W14×257	0.65	0.49	0.86
3	W14×211	0.91	0.78	1.19	W14×257	0.75	0.46	0.97
2	W14×257	0.85	0.79	1.08	W14×311	0.70	0.46	0.89
1	W14×257	0.96	0.80	1.19	W14×311	0.79	0.45	0.97

Table 4. Design DCRs for Column 2 (C2) in Three Designs of 3-Story Single-Diagonal Eccentric BRBFs												
	3S-SD-E2d-N				3S-SD-E2d-M (= Original 3S-SD-E2d)				3S-SD-E2d-X			
Story	C2 Shape	DCR_P	DCR_{SCWB}	DCR_{PM}	C2 Shape	DCR_P	DCR_{SCWB}	DCR_{PM}	C2 Shape	DCR_P	DCR_{SCWB}	DCR_{PM}
3	W14×82	0.21	0.82	0.56	W14×109	0.13	0.57	0.64	W14×132	0.10	0.46	0.52
2	W14×82	0.58	0.91	1.42	W14×109	0.35	0.61	0.96	W14×132	0.29	0.48	0.79
1	W14×82	1.03	1.69	1.87	W14×109	0.62	0.98	1.23	W14×132	0.51	0.73	1.01

Table 5. Steel Weights for Design Cases							
Group	Design Case	BRB (kips)	Column (kips)	Beam (kips)	Frame (kips)	Frame + BRB (kips)	Increase (%)
12S-SD	12S-SD-E2d-N/M†	17.39	50.61	23.42	74.03	91.42	—
	12S-SD-E2d-X	17.39	56.79	23.42	80.21	97.60	+6.76%
3S-SD	3S-SD-E2d-N	4.74	6.44	5.74	12.17	16.92	—
	3S-SD-E2d-M‡	4.74	7.65	5.74	13.39	18.13	+7.18%
	3S-SD-E2d-X	4.74	8.69	5.74	14.42	19.17	+13.30%

† Original Case 12S-SD-E2d
‡ Original Case 3S-SD-E2d

cases. Table 5 presents the steel weights for these design cases.

For 12-story frames (Table 3), the original Case 12S-SD-E2d is renamed 12S-SD-E2d-N/M, with the postfix N/M indicating that the results are derived from both Design Methods N and M. For most stories, both DCR_P and DCR_{SCWB} range from 0.8 to 1.0. Notably, for this 12-story frame, the SCWB design does not require heavier C2 members as compared to the baseline design. Case 12S-SD-E2d-X represents the results from Design Method X, as evidenced by all DCR_{PM} essentially not greater than 1.0, along with all DCR_{PM} and DCR_{SCWB} values notably lower than 1.0. As shown in Table 5, Design Method X (Case 12S-SD-E2d-X), aiming to ensure the elasticity of

individual columns, requires approximately a 7% increase in the total steel weight of the entire frame compared to the other two design methods.

For 3-story frames (Table 3), the original Case 3S-SD-E2d is renamed 3S-SD-E2d-M, with the postfix M indicating that it represents Design Method M. It should be noted that the size of C2 members (W14×109) in this design case was originally determined by the compactness requirements for moderately ductile members. This choice unintentionally results in a DCR_{SCWB} value slightly less than 1.0 for the first story, serving as a good representative for Method M. However, this design also indicates an overdesign for Design Method N, as evidenced by DCR_P values notably less than 1.0. Hence, an additional Case 3S-SD-E2d-N was developed to represent Method N, with the DCR_P (1.03) being slightly higher than 1.0 for the C2 member in first story, while the DCR_{SCWB} and DCR_{PM} values notably exceed 1.0 in the same story. Furthermore, another case, 3S-SD-E2d-X, was developed to represent Design Method X, as evidenced by its DCR_{PM} value (1.01) barely exceeding 1.0, accompanied with relatively low DCR_P and DCR_{SCWB} values for the first story. From Table 5, it can be observed that for these 3-story frames, the SCWB-based Design Method M (3S-SD-E2d-M) requires an increase of about 7% in the total steel weight as compared to the baseline Design Method N (3S-SD-E2d-N). In contrast, achieving Design Method X (3S-SD-E2d-X) requires an increase of approximately 13% in total steel weight.

Analytical Study Results

A series of NLRHA studies were conducted to evaluate the seismic performance of the five design cases representing different design methods for C2 members. For each design case, two OpenSees models (Mazzoni et al., 2006) were developed using the modeling setup illustrated in Figure 2(a). One model uses fiber beam column elements for the BRBF column elements to simulate the nonlinear response under *P-M* interaction, while the other employs elastic beam column elements for the BRBF columns to represent a pseudo case with perfectly elastic column behavior. The models are named after their respective design cases, with a postfix fib or ela to represent the use of fiber or elastic beam column elements.

Figures 18 through 20 show the MCE-level NLRHA results for these models subjected to the same two suites of 16 ground motions used for analyses on 12-story and 3-story models discussed in Section 2. These figures display the mean structural responses, including peak story drifts and peak *P-M* interaction demands on C2 members, averaged across 16 ground motions. To quantify the *P-M* interaction at each end of C2 members, two parameters were employed: the conventional DCR for *P-M* interaction (DCR_{PM}), as defined in Equation 8, and the yield ratio (YR), which evaluates the sectional yielding at the column ends. The YR is calculated as:

$$\text{YR} = \left|\frac{P_u}{P_{ye}}\right| + \left|\frac{M_u}{M_{pe}}\right| \tag{9}$$

where the axial demand, P_u, and flexural demand, M_u, are obtained from the NLRHA. The expected sectional yield axial force, P_{ye}, and the expected plastic moment, M_{pe}, are calculated as:

$$P_{ye} = R_y F_{yc} A_{gc} \tag{10}$$

$$M_{pe} = R_y F_{yc} Z_{xc} \tag{11}$$

where the factor R_y = 1.10 accounts for the material overstrength. A value of YR exceeding 1.0 indicates the sectional yielding of the column end.

The value of DCR_{PM} is determined using Equation 8 with the demands P_u and M_u obtained from the NLRHA. As C2 members experience alternating tension and compression during the NLRHA, the design axial strength ϕP_n in Equation 8 is taken as the tensile yielding strength $\phi_t P_y$ if the axial demand P_u is in tension, while the compressive strength $\phi_c P_n$ is used when P_u is compressive. Since DCR_{PM} accounts for buckling strength in compressive axial forces and incorporates the strength reduction factors (ϕ-factors) for both axial and moment capacities, its values are always greater than the YR values, which reflect sectional yielding based on the expected yield strength.

Figure 18 compares the NLRHA results between Cases 12S-SD-E2d-N/M and 12S-SD-E2d-X. For all responses shown, the overlapping results between the fib (with fiber columns) and ela (with elastic columns) models for both cases indicate no significant column yielding in either frame. As illustrated in Figure 18(a), both design cases perform well, with their story drifts remaining below the code-prescribed limit (ASCE, 2022). The story drifts of Case 12S-SD-E2d-X were slightly smaller than those of 12S-SD-E2d-N/M in several stories, specifically in the bottom two and upper five stories. This indicates that using heavier C2 members, as determined from the stricter Design Method X, does not notably enhance the performance of this 12-story eccentric BRBF compared to the frame designed with the other two methods.

Figure 18(b) shows that all the mean peak DCR_{PM} values at the ends of the C2 members in Case 12S-SD-E2d-X are less than 1.0, indicating that the objective of Design Method X is achieved. In contrast, DCR_{PM} values exceed 1.0 in only few stories (the 9th and 11th stories) in Case 12S-SD-E2d-N/M. Figure 18(b) gives the results of forces taken from the NLRHA and analyzed using Equation 8. It should be noted that a value of DCR_{PM} slightly above 1.0 from MCE-level NLRHA does not necessarily indicate column yielding and should not be directly interpreted as

failure. This is because the AISC *Seismic Provisions* generally allow the neglect of seismic moment demands (permitting some sectional yielding under *P-M* interaction) and supports an axial-only design approach for SFRS columns, which helps prevent global instability due to column buckling. The justification for applying the same principle to the C2 members in the 12-story cases is discussed below.

First, the conservative assumption of simultaneous yielding for all braces in a BRBF in column capacity design leads to an overestimate in the dynamic column axial force, as evidenced by the axial-only NLRHA DCR_P values being notably less than 1.0, as shown in Figure 11(e). These low DCR_P values indicate that the C2 members are far from column buckling.

Second, the moderate exceedance of DCR_{PM} in 12S-SD-E2d-N/M need not be of concern, as evidenced by the fact that all mean peak yield ratios are notably less than 1.0 as shown in Figure 18(c), indicating no yielding of any C2 members in 12S-SD-E2d-N/M. In addition, the peak yield ratios (denoted as Max. Response) from the 16 ground motions for the C2 members in 12S-SD-E2d-N/M are also plotted in Figure 18(c). Even these extreme column responses had yield ratios lower than 1.0. This suggests that relying solely on Design Methods N (axial-only design) or M (SCWB design) for this 12-story eccentric BRBF can effectively prevent sectional yielding under *P-M* interaction in the C2 members.

Lastly, the overestimation in axial forces in column capacity is particularly significant for high-rise buildings, which explains why the C2 members in 12-story BRBF considered, despite being designed for axial force only, do not fully consume all their capacity for axial action and retain sufficient strength to accommodate the concurrent moment demands.

Figure 19 compares the NLRHA results between Cases 3S-SD-E2d-N and 3S-SD-E2d-X. Figure 19(a) shows that all story drifts in both frames remain below the code limit (ASCE, 2022), indicating satisfactory global performance for both cases. For Case 3S-SD-E2d-X, the overlapping results between the fib and ela models for all responses indicate no notable column yielding. In this design case, the mean peak DCR_{PM} mildly exceeds 1.0 only at the top end of the first-story C2 member [Figure 19(b)] while remaining below 1.0 for the other C2 members. This suggests that, although the conventional *P-M* interaction check (Design Method X) is used for sizing C2 members, and the dynamic axial demands are generally overestimated for these members [Figure 11(f)], the proposed estimation method—assuming an even distribution of moments between column ends at a stub-to-column intersection—may underestimate the moment demands at certain ends of C2 members in a low-rise BRBF, leading to the observed exceedance of DCR_{PM} [Figure 19(b)]. Nonetheless, Figure 19(c) shows that in Case 3S-SD-E2d-X, the mean peak yield ratios are less than 1.0 for all C2 members, indicating that employing Design Method X is likely effective in preventing sectional yielding in C2 members for low-rise BRBFs.

In Case 3S-SD-E2d-N, there are clear deviations between the fib and ela models for the responses of DCR_{PM} [Figure 19(b)] and yield ratio [Figure 19(c)] for C2 members in the lower two stories. Additionally, the mean peak yield ratios exceed 1.0 for these C2 members. These findings indicate that considerable yielding occurs at the top end of the first-story column and at both ends of the

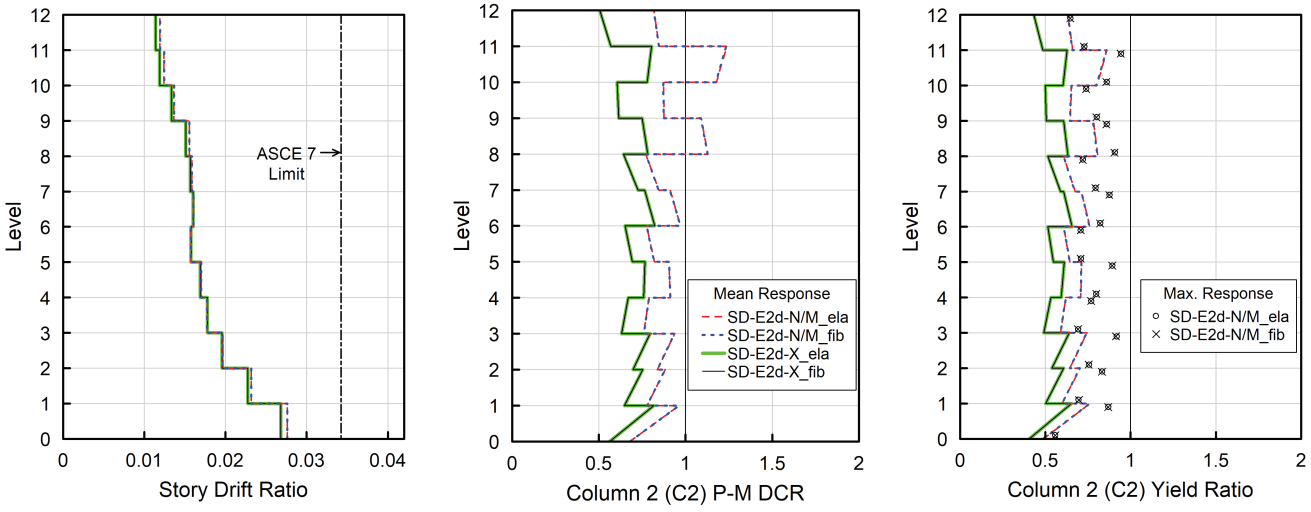

(a) Story-drift ratio

(b) P-M interaction DCR of Column 2 (C2) members

(c) Yield ratio of C2 members

Fig. 18. Comparison of NLRHA results between Design Cases 12S-SD-E2d-N/M and 12S-SD-E2d-X.

second-story column, suggesting that relying solely on the axial-only design (Design Method N) could lead to yielding of the C2 members in low-rise BRBFs. However, this sectional nonlinearity may not be of a concern, as the AISC *Seismic Provisions* (2022a) do not prohibit yielding at the SFRS column ends. Moreover, for the story drifts of Case 3S-SD-E2d-N [see Figure 19(a)], the responses from the fib and ela model are close to each other, exhibiting only minor deviations. This suggests that, despite some yielding developing in the C2 members (in the fib model), the global response of the BRBF remains very similar to that of the elastic case (in the ela model). Moreover, the story drifts of Case 3S-SD-E2d-N are only mildly greater than those of the conservatively designed Case 3S-SD-E2d-X in the bottom two stories. These indicate that employing the baseline axial-only design would not significantly reduce the global seismic performance of low-rise BRBFs, despite the potential local yielding in some C2 members.

Figure 20 shows the NLRHA results of Case 3S-SD-E2d-M in comparison to 3S-SD-E2d-X. For the story-drift response [Figure 20(a)], Case 3S-SD-E2d-M barely exceeds 3S-SD-E2d-X in the first story, accompanied with almost overlapping results between the two frames in the upper two stories. This suggests that using the SCWB-based Design Method M for C2 members can achieve a global seismic performance very close to that of the conservative Design Method X for low-rise BRBFs.

For Case 3S-SD-E2d-M, there are sight deviations between the fib and ela models for the responses of DCR_{PM} [Figure 20(b)] and the yield ratio [Figure 20(c)] of C2 members at the top of first story. In addition, the mean peak yield ratio slightly exceeded 1.0, indicating minor yielding, at the top of a first-story C2 member. It should be noted that while the SCWB design for the C2 members (3S-SD-E2d-M) requires merely about a 7% increase in total steel weight compared to the frame (3S-SD-E2d-N) determined from the axial-only design for C2 members, the yielding of C2 members in 3S-SD-E2d-M [Figure 20(c)] is significantly less than that of 3S-SD-E2d-N [Figure 19(c)]. This suggests that, for the low-rise BRBFs, employing SCWB design for the C2 members could be an efficient way to minimize the column yielding.

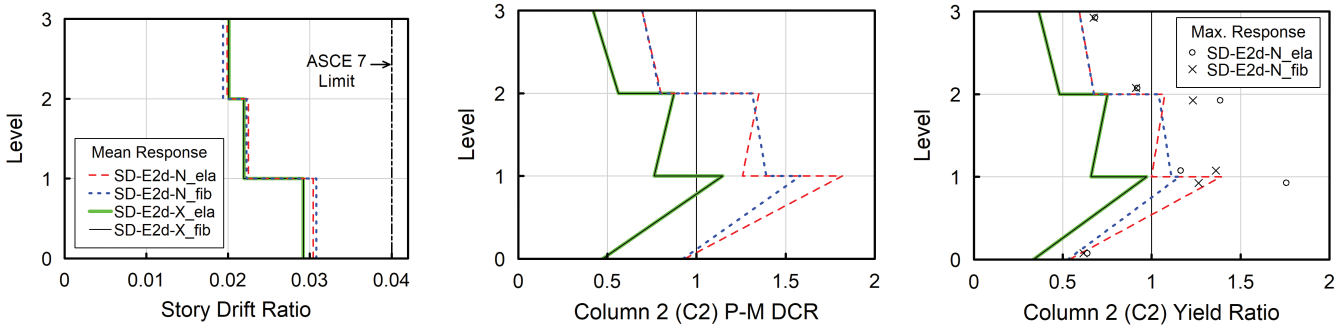

(a) Story-drift ratio *(b) P-M interaction DCR of Column 2 (C2) members* *(c) Yield ratio of C2 members*

Fig. 19. Comparison of NLRHA results between Design Cases 3S-SD-E2d-N and 3S-SD-E2d-X.

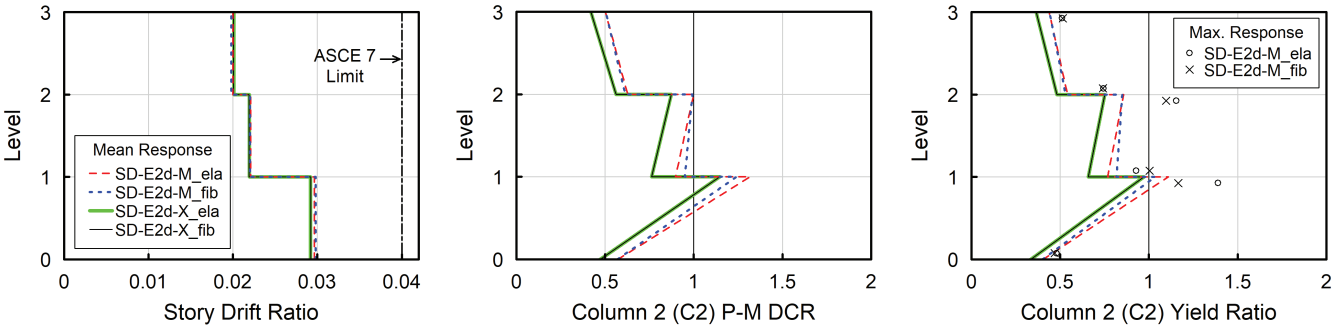

(a) Story-drift ratio *(b) P-M interaction DCR of Column 2 (C2) members* *(c) Yield ratio of C2 members*

Fig. 20. Comparison of NLRHA results between Design Cases 3S-SD-E2d-M and 3S-SD-E2d-X.

Approximate Story Shear Distribution

This section provides the estimation of the percentage of story shear resisted by the C2 members in a single-diagonal eccentric BRBF. This information can be applied to the efficient preliminary design of this type of BRBF by accounting for the contribution of C2 members to the story shear resistance. As shown in Figure 21-left, the total story shear, V_{Total}, in a typical story is the sum of the story shear components (denoted as V_{br}, V_{C1}, and V_{C2}) resisted by the braces, C1 member, and C2 member, respectively. Since the beam members are assumed to be pin connected to the C1 members, the shear in the C1 member is negligible (i.e., $V_{C1} = 0$). Thus, the total story shear can be approximated as the sum of the shears in the brace and C2 member, expressed as:

$$V_{Total} = V_{br} + V_{C1} + V_{C2} \cong V_{br} + V_{C2} \tag{12}$$

Furthermore, Figure 21-right illustrates the assumed moment diagrams for the stub and C2 member in the typical story. Because the stub behaves like a cantilever beam subjected to the vertical component of the brace axial force, P_{br}, the magnitude of bending moment at the stub end, M_{Stub}, is calculated as:

$$M_{Stub} = (P_{br} \sin\theta)e \tag{13}$$

where θ and e are the brace inclination angle and brace eccentricity, respectively.

To approximate the moment diagram in the C2 member, two assumptions are made: (1) The stub-end moment, M_{Stub}, is evenly distributed to the ends of C2 members above and below the stub-to-column joint, and (2) similar to typical SMF columns, the C2 member is assumed to bend in double curvature with an inflection point at the mid-height of the column, resulting in a linear moment diagram with equal but opposite moments at the two ends. These assumptions yield the following relationship:

$$M_{C2t} \cong M_{C2b} \cong \frac{1}{2} M_{Stub} \tag{14}$$

where M_{C2t} and M_{C2b} are the magnitudes of moments at the top and bottom ends of the C2 member, respectively. Furthermore, the shear in the C2 member, V_{C2}, can be estimated as the slope of the moment diagram, given as:

$$V_{C2} = \frac{M_{C2t} + M_{C2b}}{H} \cong \frac{2\left(\frac{1}{2} M_{Stub}\right)}{H} = \frac{M_{Stub}}{H} = \frac{(P_{br} \sin\theta)e}{H} \tag{15}$$

where H is the story height. Substituting P_{br} with $V_{br}/\cos\theta$ into Equation 15 yields:

$$V_{C2} \cong \frac{\left(\frac{V_{br}}{\cos\theta} \sin\theta\right)e}{H} = \frac{(V_{br} \tan\theta)e}{H} \tag{16}$$

Furthermore, substituting tan θ with H/b, where b is the span width tributary to the brace (calculated as the total span width L minus the brace eccentricity e, i.e., $b = L - e$), into Equation 16 gives:

$$V_{C2} \cong \frac{\left(V_{br} \frac{H}{b}\right)e}{H} = \left(\frac{e}{b}\right)V_{br} \Rightarrow \frac{V_{C2}}{V_{br}} \cong \frac{e}{b} \tag{17}$$

Thus, the ratio of story shear resisted by the C2 member to that resisted by the brace can be approximated as the ratio of the tributary span widths for each part. Finally, substituting Equation 17 into Equation 12, the following relationships can be established:

$$\frac{V_{br}}{V_{Total}} \cong \frac{b}{L} \tag{18}$$

$$\frac{V_{C2}}{V_{Total}} \cong \frac{e}{L} \tag{19}$$

These equations provide a simplified method for estimating the contributions of the brace and C2 member to the total story shear in a single-diagonal eccentric BRBF. The percentage of story shear resisted by the brace or C2

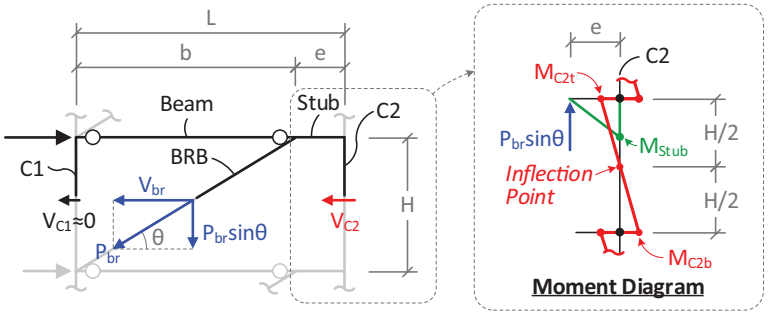

Fig. 21. Approximate analysis of story shear distribution in a typical story of a single-diagonal eccentric BRBF.

member can be approximated as the ratio or their tributary span widths to the total span width.

To validate the proposed approximation for the story shear components, V_{br} and V_{C2}, the analytical results of Design Case 12S-SD-E2d are evaluated for two levels of seismic loading. The first level is the equivalent lateral force (ELF) (ASCE, 2022), which reflects the structure's response near its elastic upper limit, while the second level corresponds to MCE, representing the peak structural response with nonlinearity during extreme seismic events. Note that, although modal response spectrum analysis (MRSA) was used for brace sizing in the case study designs, it was not applied herein to investigate story shear components at the elastic level. This is because MRSA combines modal responses using methods that inherently lose the original signs of member forces, potentially disrupting the equilibrium of internal forces among members. As a result, MRSA results are unsuitable for accurately assessing the distribution of story shear among members. Figure 22(a) shows the ELF-level story shear responses (V_{Total}, V_{br}, and V_{C2}), derived from the elastic model in ETABS (CSI, 2019) subjected to the ELF procedure. Figure 22(b) displays the MCE-level story shears, obtained from the mean peak responses of the NLRHA using the OpenSees nonlinear model (Mazzoni et al., 2006) subjected to 16 ground motions, as detailed earlier.

Figures 22(c) and 22(d) present the analysis results on the vertical distributions of the V_{br}/V_{Total} and V_{C2}/V_{Total} ratios, respectively. In each figure, the results at both the ELF and MCE levels are plotted and compared with the proposed approximation (Equations 18 or 19), denoted as Approx. The approximation reasonably matches the ELF and MCE analytical responses for all stories except for the top and bottom stories. The deviation in these two stories occurs because the assumed pattern for the moment diagram in C2 member (Figure 21-right), which applies to typical stories, may not be applicable for these atypical cases. Notably, for typical stories, the approximation predicts both V_{br}/V_{Total} and V_{C2}/V_{Total} very well at the ELF level, confirming that it offers simple and reliable measure for preliminary brace sizing while considering the contribution of C2 members to story shear resistance.

CONCLUSIONS

This paper presents the NLRHA results on the nine design cases of BRBFs with eccentricities, representing two building heights (3 and 12 stories), two bracing configurations (chevron and single-diagonal), and various eccentricities, all subjected to 16 ground motions scaled to the DBE and MCE levels. The effects of brace eccentricity on the BRBF seismic performance are also explored. Subsequently, detailed finite element modeling was performed to investigate the effects of connection geometry on beam stresses for chevron eccentric BRBFs. Lastly, the implications for the efficient design of single-diagonal eccentric BRBFs are examined, focusing on issues such as column capacity design considering moment demands and approximate story shear distribution for preliminary brace sizing.

The study supports the following conclusions:

- The NLRHA results demonstrate that the proposed design procedure [Part 1 (Li et al., 2026)] results in BRBFs with eccentricities that perform well during the DBE- and MCE-level earthquakes with story drifts staying lower than the code-prescribed limit. The results confirm the satisfactory seismic performance of BRBFs having eccentricities equal to twice the beam depth, (exceeding

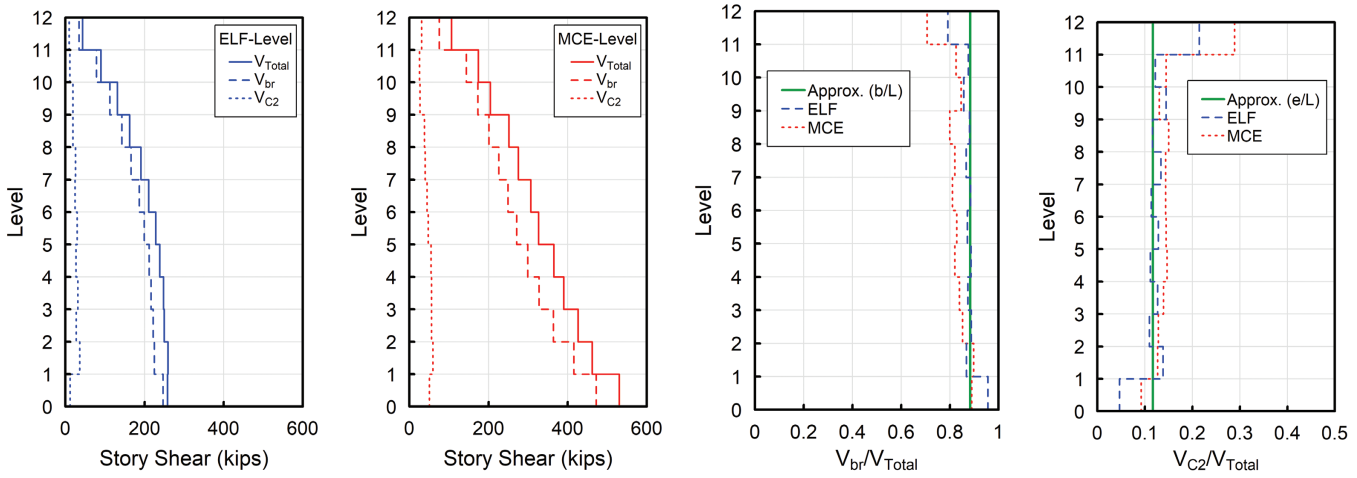

(a) ELF *(b) MCE levels and distributions* *(c) V_{br}/V_{Total}* *(d) V_{C2}/V_{Total}*

Fig. 22. Analysis results on distributions of story shear components for Case 12S-SD-E2d.

the current code limit of one beam depth), provided they are properly capacity-designed to keep the beams and columns essentially elastic (with minor column yielding allowed, provided buckling is prevented), while confining the majority of inelasticity to the BRBs. Additionally, the analytical results validate the accuracy of the proposed methods in estimating force demands for the capacity design of BRBF beams with brace eccentricity.

- In chevron BRBFs, there is a general trend of slightly increasing peak and residual drifts with eccentricity, particularly in the lower stories of the building. In contrast, single-diagonal BRBFs exhibit significantly lower peak and residual drifts in eccentric configurations compared to concentric frames, with a particularly notable reduction in residual drifts. This improvement is primarily due to the half-MRF formed by the stubs and adjacent columns, which serves as an elastic backup lateral system for single-diagonal eccentric BRBFs. This study demonstrates that by accounting for the columns' contribution to resisting story shear, single-diagonal eccentric BRBFs can be designed to be more economical than the single-diagonal concentric BRBFs, while also offering superior seismic performance. The design cases considered in this study indicate a potential reduction of approximately 3% to 5% in steel weight.
- The results of pushover analyses on detailed finite element models confirm that the proposed capacity design method on chevron BRBF beams with eccentricity, despite not accounting for the local stress distribution, would not lead to local stress concentration issues in the beam region near the brace-to-beam intersection. Additionally, the analysis demonstrates that the combined gusset configuration used for chevron BRBF beams results in lower beam web stress compared to the split gusset configuration.
- NLRHA results at the MCE level reveal that for high-rise BRBFs, the code-minimum axial-only design is sufficient to maintain C2 member elasticity due to overestimated axial demands. In low-rise BRBFs, the axial-only design may result in minor C2 member yielding without significantly affecting performance. The adapted strong column–weak beam (SCWB) design efficiently minimizes C2 member yielding in low-rise BRBFs with only a moderate increase in steel weight, while the code-beyond *P-M* interaction method achieves stringent design goal of eliminating the C2 member yielding but requires substantial additional steel.
- This study proposes an approximation of the story shear contribution for single-diagonal eccentric BRBFs, enabling hand calculations of force demand for preliminary brace sizing while accounting for the C2 members' contribution to resisting story shear. The effectiveness of this approximation is confirmed by the analysis data.

REFERENCES

AISC (2022a), *Seismic Provisions for Structural Steel Buildings*, ANSI/AISC 341-22, American Institute of Steel Construction, Chicago, Ill.

AISC (2022b), *Specification for Structural Steel Buildings*, ANSI/AISC 360-22, American Institute of Steel Construction, Chicago, Ill.

ANSYS (2022), *Ansys Mechanical Release 22.1 Help System*, ANSYS, Inc., Canonsburg, Pa.

ASCE (2022), *Minimum Design Loads and Associated Criteria for Buildings and Other Structures*, ASCE/SEI-7-22, American Society of Civil Engineers, Reston, Va.

ATC (2009), *Quantification of Building Seismic Performance Factors,* FEMA P695, Federal Emergency Management Agency, Washington D.C.

CSI (2019), *CSI Analysis Reference Manual for SAP2000, ETABS, SAFE and CSiBridge,* Computers and Structures, Inc., Berkeley, Calif.

Fortney, P.J. and Thornton, W.A. (2017), "The Chevron Effect and the Analysis of Chevron Beams—A Paradigm Shift," *Engineering Journal*, Vol. 54, No. 4, pp. 263–296.

Gholami, M., Zare, E., Gorji Azandariani, M., and Moradifard, R. (2021), "Seismic Behavior of Dual Buckling-Restrained Steel Braced Frame with Eccentric Configuration and Post-Tensioned Frame System," *Soil Dynamics and Earthquake Engineering*, Vol. 151, No. 2021, pp. 106977.

Hariri, B. and Christopoulos, C. (2024), "Numerical Hybrid Simulation Assessment of E-BRBF and E-FBF Systems for Mitigating P-Delta Effects and Enhancing Post-Earthquake Performance," *Earthquake Engineering & Structural Dynamics*, Vol. 53, No. 12, pp. 3754–3774.

Hosseini, S.M. and Amiri, G.G. (2017), "Successive Collapse Potential of Eccentric Braced Frames in Comparison with Buckling-Restrained Braces in Eccentric Configurations," *International Journal of Steel Structures*, Vol. 17, No. 2, pp. 481–489.

Lejano, B.A. and Mas, M.J.S. (2017), "Numerical Study on the Effect of Structural Parameters on the Behavior of BRBF-E," The Third International Conference on Civil Engineering Research (ICCER), Surabaya, Indonesia.

Li, C.-H., Richards, P.W., Saxey, B.W., and Richards, H.L. (2026), "Seismic Design and Performance of Buckling Restrained Brace Frames with Eccentric Brace Configurations Part 1: Design Procedures and Case Studies," *Engineering Journal*, AISC, Vol. 63, No. 1, pp. 49–74.

Lignos, D.G., Putman, C., and Krawinkler, H. (2013), "Seismic Assessment of Steel Moment Frames Using Simplified Nonlinear Models," in *Computational Methods in Applied Sciences* (Vol. 2, pp. 91–109), Springer Nature.

Liu, J. and Astaneh-Asl, A. (2000), "Cyclic Testing of Simple Connections Including Effects of Slab," *Journal of Structural Engineering*, Vol. 126, No. 1, pp. 32–39.

Liu, J. and Astaneh-Asl, A. (2004), "Moment–Rotation Parameters for Composite Shear Tab Connections," *Journal of Structural Engineering*, Vol. 130, No. 9, pp. 1371–1380.

Lowes, L.N., Mitra, N., and Altoonash, A. (2003), *A Beam-Column Joint Model for Simulating the Earthquake Response of Reinforced Concrete Frames*, Pacific Earthquake Engineering Research Center, Berkeley, Calif.

Mazzoni, S., McKenna, F., Scott, M., and Fenves, G. (2006), *OpenSees Command Language Manual,* Pacific Earthquake Engineering Research Center, Berkeley, Calif. http://opensees.berkeley.edu/wiki/index.php/Command_Manual

NIST (2010), *Evaluation of the FEMA P-695 Methodology for Quantification of Building Seismic Performance Factors*, GCR 10-917-8, National Institute of Standards and Technology, Gaithersburgh, Md.

NIST (2017), *Recommended Modeling Parameters and Acceptance Criteria for Nonlinear Analysis in Support of Seismic Evaluation*, GCR 17-917-45, National Institute of Standards and Technology, Gaithersburg, Md.

PEER. (2006), *PEER NGA Database*, Pacific Earthquake Engineering Center, Berkeley, Calif.

Prinz, G.S. and Richards, P.W. (2012), "Seismic Performance of Buckling-Restrained Braced Frames with Eccentric Configurations," *Journal of Structural Engineering*, Vol. 138, No. 3, pp. 345–353.

Sabelli, R. and Arber, L. (2017), "Design of Chevron Gusset Plates," *SEAOC Convention Proceedings*, San Diego, Calif.

Shakib, H. and Safi, R. (2012), "Behavior Evaluation of the Eccentric Buckling-Restrained Braced Frame under the Near-Fault Ground Motions," 15th World Conference on Earthquake Engineering, Lisbon, Portugal.

Vayda, P.T. (2015), *Comparative Analysis of Buckling-Restrained Braced Frames in Eccentric Configurations (BRBF-Es) and Eccentrically Braced Frames (EBFs)*, University of Arkansas, Fayetteville, Ark.

See Appendix on next page

APPENDIX

Ground motion records for the response history analysis were taken from the PEER NGA database (PEER, 2006). Tables A.1 and A.2 summarize the records and scaling factors used for the analyses of the 12- and 3-story frames, respectively.

Table A.1. Gound Motions for 12-Story Models

Ground Motion Number	Earthquake	Station	PEER-NGA Record Information		DBE Scale Factor	MCE Scale Factor
			Record Sequence Number	File Name (Horizontal Record)		
1	1994 Northridge	Canyon Country—W Lost Cany	960	NORTHR/LOS000	1.4511	2.1767
2	1994 Northridge	Canyon Country—W Lost Cany	960	NORTHR/LOS270	1.4525	2.1787
3	1999 Hector Mine	Hector	1787	HECTOR/HEC000	2.3605	3.5407
4	1999 Hector Mine	Hector	1787	HECTOR/HEC090	1.6594	2.4891
5	1979 Imperial Valley	Delta	169	IMPVALL/H-DLT262	2.5082	3.7623
6	1979 Imperial Valley	Delta	169	IMPVALL/H-DLT352	1.9454	2.9180
7	1995 Kobe (Japan)	Shin-Osaka	1116	KOBE/SHI000	1.9341	2.9012
8	1995 Kobe (Japan)	Shin-Osaka	1116	KOBE/SHI090	2.6483	3.9725
9	1999 Kocaeli (Turkey)	Duzce	1158	KOCAELI/DZC180	1.0021	1.5031
10	1999 Kocaeli (Turkey)	Duzce	1158	KOCAELI/DZC270	1.1035	1.6552
11	1992 Landers	Yermo Fire Station	900	LANDERS/YER270	1.0399	1.5598
12	1992 Landers	Yermo Fire Station	900	LANDERS/YER360	1.8081	2.7122
13	1987 Superstition Hills	El Centro Imp. Co. Cent	721	SUPERST/B-ICC000	1.8399	2.7598
14	1987 Superstition Hills	El Centro Imp. Co. Cent	721	SUPERST/B-ICC090	2.1067	3.1600
15	1999 Chi Chi (Taiwan)	CHY101	1244	CHICHI/CHY101-E	0.9894	1.4841
16	1999 Chi Chi (Taiwan)	CHY101	1244	CHICHI/CHY101-N	0.7959	1.1938

Table A.2. Gound Motions for 3-Story Models						
Ground Motion Number	Earthquake	Station	PEER-NGA Record Info.		DBE Scale Factor	MCE Scale Factor
			Record Sequence Number	File Name (Horizontal Record)		
1	1994 Northridge	Beverly Hills—14145 Mulhol	953	NORTHR/MUL009	1.0662	1.5994
2	1994 Northridge	Beverly Hills—14145 Mulhol	953	NORTHR/MUL279	0.8999	1.3499
3	1994 Northridge	Canyon Country—W Lost Cany	960	NORTHR/LOS000	1.4809	2.2214
4	1994 Northridge	Canyon Country—W Lost Cany	960	NORTHR/LOS270	1.0129	1.5194
5	1999 Düzce (Turkey)	Bolu	1602	DUZCE/BOL000	0.7725	1.1587
6	1999 Düzce (Turkey)	Bolu	1602	DUZCE/BOL090	0.8931	1.3396
7	1999 Hector Mine	Hector	1787	HECTOR/HEC000	1.9542	2.9313
8	1999 Hector Mine	Hector	1787	HECTOR/HEC090	1.4777	2.2166
9	1995 Kobe (Japan)	Shin-Osaka	1116	KOBE/SHI000	1.6243	2.4364
10	1995 Kobe (Japan)	Shin-Osaka	1116	KOBE/SHI090	2.0485	3.0728
11	1992 Landers	Yermo Fire Station	900	LANDERS/YER270	1.4278	2.1417
12	1992 Landers	Yermo Fire Station	900	LANDERS/YER360	1.5792	2.3688
13	1999 Chi Chi (Taiwan)	CHY101	1244	CHICHI/CHY101-E	1.2059	1.8089
14	1999 Chi Chi (Taiwan)	CHY101	1244	CHICHI/CHY101-N	0.9942	1.4913
15	1999 Chi Chi (Taiwan)	TCU045	1485	CHICHI/TCU045-E	1.4831	2.2246
16	1999 Chi Chi (Taiwan)	TCU045	1485	CHICHI/TCU045-N	1.4307	2.1460